



HAL
open science

Controls on Polar Southern Ocean Deep Chlorophyll Maxima: Viewpoints From Multiple Observational Platforms

Philip W. Boyd, David Antoine, Kimberley Baldry, Marin Cornec, Michael Ellwood, Svenja Halfter, Leo Lacour, Pauline Latour, Robert F. Strzepek, Thomas W. Trull, et al.

► **To cite this version:**

Philip W. Boyd, David Antoine, Kimberley Baldry, Marin Cornec, Michael Ellwood, et al.. Controls on Polar Southern Ocean Deep Chlorophyll Maxima: Viewpoints From Multiple Observational Platforms. *Global Biogeochemical Cycles*, 2024, 38, 10.1029/2023GB008033 . insu-04786611

HAL Id: insu-04786611

<https://insu.hal.science/insu-04786611v1>

Submitted on 17 Nov 2024

HAL is a multi-disciplinary open access archive for the deposit and dissemination of scientific research documents, whether they are published or not. The documents may come from teaching and research institutions in France or abroad, or from public or private research centers.

L'archive ouverte pluridisciplinaire **HAL**, est destinée au dépôt et à la diffusion de documents scientifiques de niveau recherche, publiés ou non, émanant des établissements d'enseignement et de recherche français ou étrangers, des laboratoires publics ou privés.



Distributed under a Creative Commons Attribution - NonCommercial - NoDerivatives 4.0 International License

Global Biogeochemical Cycles®




RESEARCH ARTICLE

10.1029/2023GB008033

Controls on Polar Southern Ocean Deep Chlorophyll Maxima: Viewpoints From Multiple Observational Platforms

Key Points:

- Coupled Deep Chlorophyll Maxima (DCM) and Deep Biomass Maxima (DBM) subsurface features in the polar Southern Ocean are formed while mixed layer chlorophyll is not depleted
- These subsurface features are dominated by large diatoms, and persist for around 3 months before declining due to low light conditions
- DCM/DBMs photosynthetically fix low levels of carbon but their longevity results in a substantial amount of carbon export to depth

Philip W. Boyd^{1,2,3} , David Antoine⁴, Kimberley Baldry¹, Marin Cornec⁵, Michael Ellwood^{6,7}, Svenja Halfter^{1,8}, Leo Lacour^{1,9}, Pauline Latour^{1,3}, Robert F. Strzepek^{1,2}, Thomas W. Trull¹⁰, and Tyler Rohr^{1,10}

¹Institute for Marine and Antarctic Studies, University of Tasmania, Hobart, TAS, Australia, ²Australian Antarctic Program Partnership (AAPP), Institute for Marine and Antarctic Studies, University of Tasmania, Hobart, TAS, Australia, ³ARC Australian Centre for Excellence in Antarctic Sciences (ACEAS), University of Tasmania, Hobart, TAS, Australia, ⁴School of Earth & Planetary Sciences, Curtin University, Perth, WA, Australia, ⁵School of Oceanography, University of Washington, Seattle, WA, USA, ⁶Research School of Earth Sciences, Australian National University, Canberra, ATC, Australia, ⁷Australian Centre for Excellence in Antarctic Science (ACEAS), Australian National University, Canberra, ATC, Australia, ⁸NIWA Wellington, Wellington, New Zealand, ⁹Laboratoire d'Océanographie de Villefranche, CNRS & Sorbonne Université, LOV, Villefranche-sur-Mer, France, ¹⁰CSIRO Environment, Hobart, TAS, Australia

Supporting Information:

Supporting Information may be found in the online version of this article.

Correspondence to:

P. W. Boyd,
Philip.Boyd@utas.edu.au

Citation:

Boyd, P. W., Antoine, D., Baldry, K., Cornec, M., Ellwood, M., Halfter, S., et al. (2024). Controls on polar southern ocean deep chlorophyll maxima: Viewpoints from multiple observational platforms. *Global Biogeochemical Cycles*, 38, e2023GB008033. <https://doi.org/10.1029/2023GB008033>

Received 13 NOV 2023

Accepted 1 MAR 2024

Abstract Deep Chlorophyll Maxima (DCMs) are ubiquitous in low-latitude oceans, and of recognized biogeochemical and ecological importance. DCMs have been observed in the Southern Ocean, initially from ships and recently from profiling robotic floats, but with less understanding of their onset, duration, underlying drivers, or whether they are associated with enhanced biomass features. We report the characteristics of a DCM and a Deep Biomass Maximum (DBM) in the Inter-Polar-Frontal-Zone (IPFZ) south of Australia derived from CTD profiles, shipboard-incubated samples, a towbody, and a BGC-ARGO float. The DCM and DBM were ~20 m thick and co-located with the nutricline, in the vicinity of a subsurface ammonium maximum characteristic of the IPFZ, but ~100 m shallower than the ferricline. Towbody transects demonstrated that the co-located DCM/DBM was broadly present across the IPFZ. Large healthy diatoms, with low iron requirements, resided within the DCM/DBM, and fixed up to 20 mmol C m⁻² d⁻¹. The BGC-ARGO float revealed that DCM/DBM persisted for >3 months. We propose a dual environmental mechanism to drive DCM/DBM formation and persistence within the IPFZ: sustained supply of both recycled iron within the subsurface ammonium maxima, and upward silicate transport from depth. DCM/DBM cell-specific growth rates were considerably slower than those in the overlying mixed layer, implying that phytoplankton losses such as herbivory are also reduced, possibly because of heavily silicified diatom frustules. The light-limited seasonal termination of the observed DCM/DBM did not result in a “diatom dump”, rather ongoing diatom downward export occurred throughout its multi-month persistence.

Plain Language Summary Deep Chlorophyll and Deep Biomass Maxima are typically observed in the low latitude oceans where they contribute to regional ecology and biogeochemistry. They are cryptic features not observable from satellites. They are being more frequently observed in the Southern Ocean due to increased deployment of robotic profilers. The mechanisms that lead to their formation are not well understood in the Southern Ocean. Little is known about their seasonality or biogeochemical role. We use multiple observational platforms to address these issues.

1. Introduction

Deep Chlorophyll Maxima (DCMs) were initially observed in the low-latitude oligotrophic ocean, where they were conspicuous in vertical fluorescence profiles at the base of the seasonal thermocline and upper portion of the nitracline (Cullen, 1982, 2015; Hogle et al., 2018). These features have subsequently been observed in other basins, including the Southern (S.) Ocean (Holm-Hansen and Hewes, 2004; Parslow et al., 2001; Trull et al., 2001), during oceanographic surveys such as the World Ocean Circulation Experiment (WOCE). In the last decade, the deployment of robotic profiling floats has revealed that DCMs are widespread features across the global ocean (Cornec, Claustre, et al., 2021). Frequent sampling by such floats has provided insights into the seasonality of DCMs (Bock et al., 2022; Cornec, Claustre, et al., 2021).

© 2024 The Authors.

This is an open access article under the terms of the [Creative Commons Attribution-NonCommercial License](https://creativecommons.org/licenses/by-nc/4.0/), which permits use, distribution and reproduction in any medium, provided the original work is properly cited and is not used for commercial purposes.

DCMs are best characterized in the low-latitude ocean, often using a comparison of physical, chemical and bio-optical vertical profiles (Cullen, 2015). Other insights have come from discrete sampling of the subsurface features and subsequent shipboard manipulation experiments to elucidate their environmental controls (Hogle et al., 2018; Hopkinson & Barbeau, 2008). This multi-faceted research allowed the determination of several factors controlling DCMs: a well-stratified seasonally stable thermocline and sufficient irradiance for phytoplankton growth along with contact with the nitracline, often via internal waves (Cullen, 2015). Under the classification of DCMs developed by Cornec, Claustre, et al. (2021), these low-latitude persistent features are termed Typical Stable Water Systems (see Cullen, 2015). Low-latitude DCM habitats are dominated by phytoplankton groups such as picophytoplankton (Cullen, 2015). These communities typically exploit the episodic supply of additional nutrients and hence can play both an important ecological and biogeochemical role, such as fueling additional downward export flux (Pollehne et al., 1993).

In the last decade, the deployment of profiling robotic floats with a range of bio-optical sensors (such as chlorophyll fluorescence and backscatter) in oligotrophic and other oceanic regions has enhanced our ability to classify these subsurface features (Cornec, Claustre, et al., 2021; Strutton et al., 2023). Some DCMs have co-located Deep Biomass Maxima (DBMs), whereas others have no DBM but result from a photoacclimatory increase in cellular chlorophyll to harvest light at depth. The ocean-wide coverage of robotic profiling floats has also provided insights into the geographical distribution and typology of DCM/DBMs (Bock et al., 2022; Cornec, Claustre, et al., 2021).

For other DCM categories reported in Cornec, Claustre, et al. (2021), a diverse range of drivers has been developed from both observational and experimental studies, that differ from the classical model of light/nitrate and picophytoplankton for the oligotrophic ocean (Cullen, 2015). For example, (new) iron supply and light are key controls on the resident picoeukaryotes and diatoms in DCM/DBMs in the North Pacific (Hopkinson & Barbeau, 2008). The supply of regenerated nutrients has also been invoked as a driver for (diatom-dominated) DCM/DBMs in the Mediterranean Sea (Marañón et al., 2021). For other regional diatom-dominated DCM/DBMs, silicate and/or iron supply from underlying waters have been proposed as candidate drivers (Allen et al., 2005; Yool & Tyrrell, 2003). Mesoscale eddies can also play a role in DCM/DBM formation (Cornec, Laxenaire, et al., 2021; Strutton et al., 2023). In some oligotrophic regions, photoacclimation alone can be the driver that underpins the presence of DCMs (Barbieux et al., 2019). For the S. Ocean, Pinkerton et al. (2021), using data from three BGC-ARGO floats, advocate using a new metric - the irradiance at the base of the mixed layer - to explain the magnitude of DCMs.

In the S. Ocean, proposed drivers of DCM/DBM formation include silicate resupply from the nutricline (Parslow et al., 2001), and “irregular fertilization” by iron (Cornec, Claustre, et al., 2021), potentially via eddies (Uchida et al., 2020) since the DCM/DBM depth is typically shallower than that of the ferricline (Klunder et al., 2011). S. Ocean DCM/DBMs also differ from those in other regions in that they are only observed - by floats - over a few months during austral summer (see Figure 4 in Cornec, Claustre, et al., 2021) and their magnitudes are typically smaller (see Figures S20 and S21 in Cornec, Claustre, et al., 2021). These puzzling features have been classified as “Ghost Zones” by Cornec, Claustre, et al. (2021) because a suite of outstanding questions remains regarding the drivers of initiation, longevity, fate, and biogeochemical roles of S. Ocean DCM/DBMs. Here, we employ 3 distinctive approaches: ship Conductivity–Temperature–Depth (CTD) profiles and rosette sampling, towbody surveys, and high temporal resolution BGC-ARGO profiles to jointly explore the underpinning mechanisms, spatial bounds, environmental controls, links to the DBM, and seasonality of the S. Ocean DCM. This, in turn, enables us to begin to probe the biogeochemical and ecological roles of S. Ocean DCM/DBMs.

2. Materials and Methods

The data presented here were obtained during the 42-day SOLACE (Southern Ocean Large Areal Carbon Export) voyage on the RV Investigator (IN2020_V08) from 6 December 2020 to 15 January 2021 to the S. Ocean along with several months of observations from a robotic profiling BGC-ARGO float deployed at a polar site (55.48°S 138.5°E) during this voyage. SOLACE occupied three sites, one in the subantarctic (47.1°S, 141.4°E) near the Southern Ocean Time Series (SOTS) station, and two south of the Polar Front (55.8°S 138.5°E (24 to 31 December 2020), 57.8°S 141.5°E (1–11 January), Figure S1 in Supporting Information S1). The results presented here focus only on the two polar sites, both sampled in a quasi-Lagrangian mode following the deployment of a holey-sock drogue at the mid-depth of the seasonal mixed layer. The drogue drift trajectory over 10 days at the

55.8°S site is presented in Figure S2 in Supporting Information S1. The trajectory was typical of the low advective regimes we sought on SOLACE, and was similar to that observed at the southern site.

At each polar site, vertical oceanographic profiles were obtained using a Sea-Bird SBE911-plus CTD unit (conductivity, temperature, and depth) that was linked to a calibrated fluorometer (Chelsea Aqua-Tracker Mk3), oxygen (SBE 43 electrode), photosynthetically active radiation (i.e., PAR, Biospherical Laboratories) and transmissometer (Wetlabs C-Star 700 nm) sensors. Mixed Layer Depths were computed for each CTD profile using the mean of a density threshold and density gradient algorithm. For the threshold, we followed Boyer Montegut et al.'s (2004) criteria (via Holte and Talley, 2009): a density difference of 0.03 kg m^{-3} referenced to the closest measurement to 10 dbar. For the mixed layer gradient, we followed Dong et al. (2007) (via Holte and Talley, 2009) where the gradient criterion was $0.0005 \text{ kg m}^{-3} \text{ dbar}^{-1}$.

For CTD profiles of chlorophyll fluorescence, generally daytime values (exhibiting NPQ (Non Photochemical Quenching) were interpolated between dark (i.e., nighttime or deep) values. For the continuous underway fluorescence measured while in the vicinity of each site, daytime values were interpolated because nighttime measurements occur close in space and time (Thomalla et al., 2018). However, for the CTD profiles, nighttime profiles were only used if they were obtained within 24 hr and 50 km of the relevant daytime profile. In this scenario, all nearby nighttime profiles were averaged to create a representative mean night profile. Daytime values from above the euphotic depth, which were lower than the mean nighttime profile, were replaced with those from the mean nighttime profile after Thomalla et al. (2018). The euphotic depth was calculated as the in situ depth where PAR is 1% of surface ocean values (Kirk, 1994). If there were no nearby nighttime profiles to interpolate over a given daytime cast, then all fluorescence values above the maximum value within the euphotic zone were assigned equal to that value, following Xing et al. (2012) and Biermann et al. (2015). Profiles were subsequently smoothed with a 5 m moving average to remove high frequency variability and the associated risk of over-correction (Xing et al., 2012).

Discrete chlorophyll samples were used to fit to a linear regression against the corresponding in situ measurements, both underway and on the CTD. These relationships were used to correct between instruments such that all measurements were corrected toward the shipboard fluorometer. For CTD values, this relationship was computed independently at SOTS and the two combined Southern sites with site-specific correction factors were used. For underway values, a single correction factor was computed, as all discrete underway sampling was done in transit, between sites.

The CTD and associated instruments were mounted within the frame of a 24 bottle (12 L) rosette sampler. The CTD sensor package was calibrated after Kwong et al. (2020). Seawater was sampled from the rosette at selected depths for nutrients and rate measurements (including iron uptake, see later). Dissolved macronutrients were analyzed following procedures in Rees et al. (2018). Seawater samples for trace metal and isotope determination were collected using acid-cleaned Teflon-coated, externally sprung, 12 L Niskin bottles attached to an autonomous rosette equipped with a Sea-Bird SBE911-plus CTD unit following methods detailed in Ellwood et al. (2020a, b). Particulate trace metal samples were collected in situ onto acid-leached $0.2\text{-}\mu\text{m}$ PVDF (142 mm diameter) filters (Sterlitech) using six large-volume dual-head pumps (McLane Research Laboratories) deployed at various water depths (Ellwood et al., 2020a, 2020b). Elemental analysis for dissolved and particulate trace metals followed procedures in Ellwood et al. (2020b). Discrete Particulate Organic Carbon (POC) samples were analyzed following Trull et al. (2018). The POC data were used to calibrate the CTD transmissometer (Figure S3 in Supporting Information S1). In situ values from the instrument were averaged across all depths within 5 m (above or below) of the Niskin bottles from which the discrete POC samples were obtained. Beam attenuation, c (m^{-1}) was computed from the transmissometer as

$$c = -(1/.25) \times \ln(\text{trans}/100)$$

where trans is the beam transmittance (%). The beam attenuation from particulates (c_p) is estimated by subtracting the attenuation due to the intrinsic properties of seawater (c_{sw}),

$$c_p = c - c_{sw}$$

c_{sw} is set using the minimum value measured by the sensor at depth, assuming particle-free seawater. An estimate of the proportion of detrital (i.e., non-phytoplankton) POC was obtained by assuming a carbon to chlorophyll ratio of 30 (g:g) in living phytoplankton (Strutton et al., 2023), such that

$$\text{Detrital Fraction} = (\text{POC} - 30 \times \text{chlorophyll}).$$

Water from the trace metal rosette was also obtained for biological and biogeochemical metrics. Extracted Chl, photochemical efficiency (F_v/F_m), and the functional absorption cross-section (σ_{PSII} ; nm^2 reaction center (RC)⁻¹) of photosystem II (PSII) were measured by Boyd et al. (2022). Biogenic silica (BSi) was determined by measuring silicic acid spectrophotometrically after converting BSi to silicic acid through leaching with 0.1 M sodium hydroxide at 85°C for 2.25 hr (Paasche, 1973). Samples from multiple depths across the seasonal mixed layer and DCM/DBM were incubated in shipboard temperature-controlled ($\pm 0.5^\circ\text{C}$) seawater incubators with light depths mimicked using a range of neutral density screening. Daily rates of Net Primary Production (NPP) and iron uptake were measured for 0.2–2 μm , 2–20 μm , >20 μm size fractions and the community (>0.2 μm) following procedures in Boyd et al. (2022). NPP was calculated from non-titanium-washed filters, as titanium decreased carbon (C) uptake rates by ~15%. However, iron (Fe) and Fe:C uptake rates were calculated using titanium-washed Fe and C samples, and so are intracellular. Six light depths were chosen to provide coverage across the mixed layer and within the underlying DCM. The 1% I_0 (surface irradiance) ranged from 83 to 92 m depth (with an attenuation coefficient (K_d) ~0.05).

The Triaxus towbody (MacArtney A/S, Esbjerg, Denmark) was towed at ~9 knots (using ~800 m of conducting core cable). It was undulated from ~15 to 200 m depth to observe the co-located DCM and DBM. We investigated measurements from a suite of sensors on the towbody including nitrate (SUNA UV-spectrometer, SBE), oxygen (SBE 43 electrodes plumbed in line with the CTD intakes) duplicate Sea-Bird SBE911 CTDs and a calibrated Sea-Bird ECO-Triplet FLBBCD2K measuring chlorophyll fluorescence (470/695 nm excitation/emission), optical backscatter (700 nm), and dissolved organic matter fluorescence (370/460 nm—not discussed here) (Sea-Bird Electronics, Bellevue, USA). All data from these instruments were integrated over 2-s intervals. The estimation of the mixed layer depth was as for the CTD profiles. Profiles from each up/down Triaxus profile were smoothed with a 10 m moving average. A DCM was identified when the maximum chlorophyll concentration was below the mixed layer depth (MLD) and >10% greater than the mixed layer depth chlorophyll mean value. The thickness of the DCM is based on the region with at least 50% of the difference between the MLD mean and maximum chlorophyll value. This method was also applied to the identification of a DBM using the POC field measured by the transmissometer using the same calibration as described for the CTD. We employ the term “deep enhancement”, which is defined as the percentage increase of the DCM mean (averaged across the thickness of DCM) relative to the MLD mean (see Figure S4 in Supporting Information S1). Deep enhancement of POC and C:Chlorophyll is computed within the DCM rather than independently defining a DBM and D(C:Chl)M, respectively, with potentially different vertical boundaries.

A BGC-ARGO robotic profiling float (Provor-CTS5 float (NKE)), WMO 5906624, was deployed at the 56°S site during our voyage. It had the following sensor constellation: a SBE41 CTD (Sea-Bird); an ECO-Triplet composed of a chlorophyll *a* fluorometer (excitation at 470 nm; emission at 695 nm), a Colored Dissolved Organic Matter (CDOM) fluorometer, and an optical backscattering sensor at 700 nm and angle of 124° (bbp); an OCR-504 (Satlantic) radiometer measuring PAR integrated over 400–700 nm; a SUNA-V2 nitrate sensor (Satlantic); a Seafet pH sensor (Sea-Bird); an Andraea optode-4330 for dissolved oxygen, and an Underwater Vision Profiler (UVP) version 6. The float was programmed to profile every 2–4 days from December to late March and thereafter every 10 days with parking depths of 500 or 1,000 m. Following Argo protocols, hydrological data collected by the SBE41 Seabird CTD sensors were processed and quality-controlled, as described by Wong et al. (2023). Bio-optical adjusted data were used after quality-control following Schmechtig et al. (2014) for chlorophyll fluorescence, and Schmechtig et al. (2019) for the bbp. Chlorophyll *a* values were multiplied by a S. Ocean-specific correction factor of 0.3 following Ardyna et al. (2019). The bbp was converted to POC using the S. Ocean-specific relationship reported in Johnson et al. (2017). Phytoplankton carbon (C) was then derived assuming a contribution to POC of 30% (Behrenfeld et al., 2005). Chlorophyll *a* and bbp were partitioned into four components following Briggs et al. (2020): small, labile fluorescing (chl_{a_s}) and backscattering (bbp_s) particles; and large, fast-sinking fluorescing (chl_{a_l}) and backscattering (bbp_l) particles. The division between small and large corresponds approximately to a particle chlorophyll content of 60 pg for chl_{a_s} versus chl_{a_l} and a particle

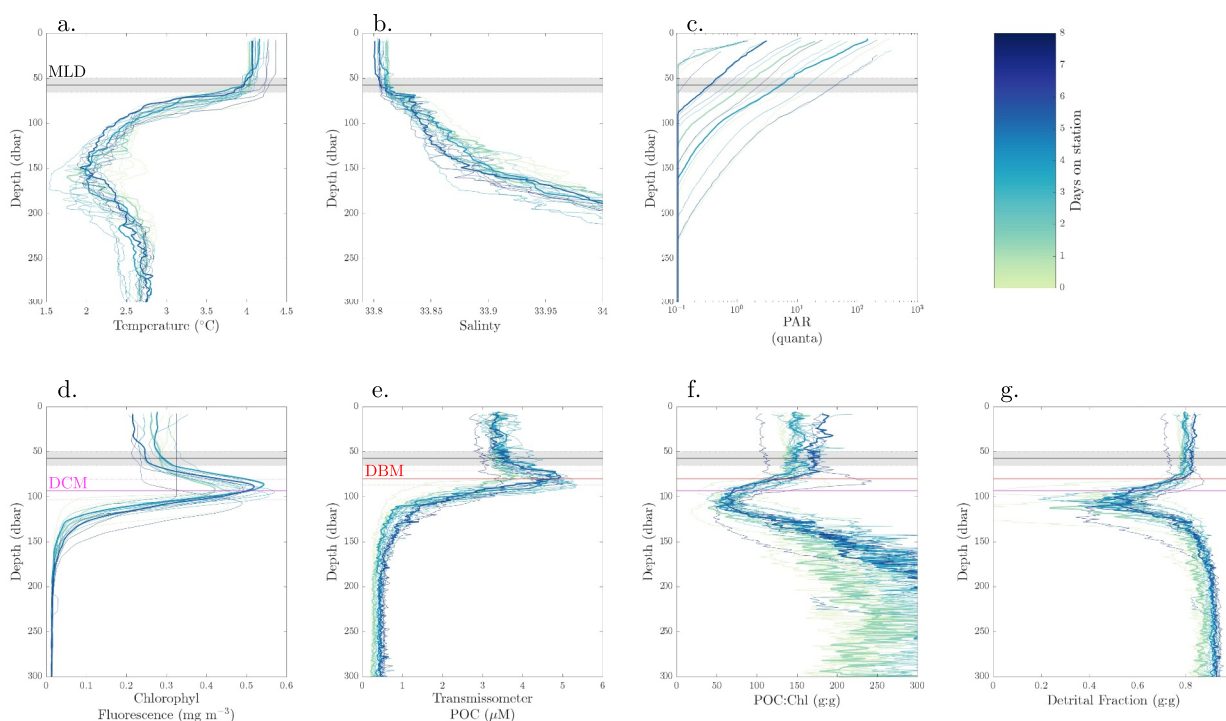


Figure 1. Vertical profiles for the 56°S station from calibrated CTD sensors. (a) Temperature, (b) salinity, (c) irradiance (PAR), (d) Chl fluorescence, (e) transmissometer POC, (f) POC:Chl ratio, (g) proportion of detrital fraction. MLD denotes the mean Mixed Layer Depth for all profiles with ± 1 standard deviation. Dashed lines labeled DCM and DBM denote the mean position of these subsurface features. Dotted lines in (d) and (e) denote the mean vertical extent of each feature. In panels (d) and (e), the location of each subsurface feature is identified by smoothing each profile with a 10 m moving mean and then identifying the maximum. The maximum is 10% larger than the mixed layer mean value to qualify. The vertical extent of each feature is defined as the region with 50% of the difference between the MLD mean and maximum concentration. Days since arriving at the 56°S station on 24 December 2020, for each profile are denoted on the color bar. Chlorophyll profiles with uniform surface values in the euphotic zone were obtained during day-casts and have been NPQ corrected.

diameter of 100 μm for bbp_2 versus bbp_1 . Data are available through the Coriolis database (<ftp://ftp.ifremer.fr/ifremer/argo>; Argo, 2000). The float data were collected and made freely available by the International Argo Program and the national programs that contribute to it (<https://argo.ucsd.edu>, <https://www.ocean-ops.org>). The Argo Program is part of the Global Ocean Observing System.

3. Results

3.1. Ship-Based Sampling

A combination of data from CTD profiles and discrete chemical sampling provides a broader oceanographic context with which to interpret the location of the DCM/DBM feature. Two sites were occupied for multiple days at 55.48°S 138.34°E (hereafter referred to as 56°S) and further to the SE at 58°S 141°E (hereafter referred to as 58°S) in late December 2020 and early January 2021 during the SOLACE voyage (Figure S1 in Supporting Information S1). Each site was selected using 3-day composite satellite maps of chlorophyll concentrations overlaid on sea surface height anomaly (Figure S1b in Supporting Information S1), and low advective sites with elevated chlorophyll stocks were sought. At 56°S, the water column was characterized by temperature/salinity properties of the IPFZ (Parslow et al., 2001), including a temperature minimum (Tmin) layer between 100 and 300 m depth (Figure 1a).

A DCM was evident at 56°S as a >20 m thick feature in chlorophyll fluorescence (Figure 1d) co-located with the upper strata of the Tmin layer and associated with low underwater irradiances (Figures 1a and 1c). The DCM was co-located with a DBM across all 10 profiles, indicative of biomass accumulation (Figure 1e); however, a coincident decrease in the C:Chlorophyll ratio points to photoacclimation at depth as well (Figure 1f). The proportion of detrital POC was ~ 0.9 in the mixed layer and decreased to ~ 0.7 in DCM/DBM (Figure 1g). This

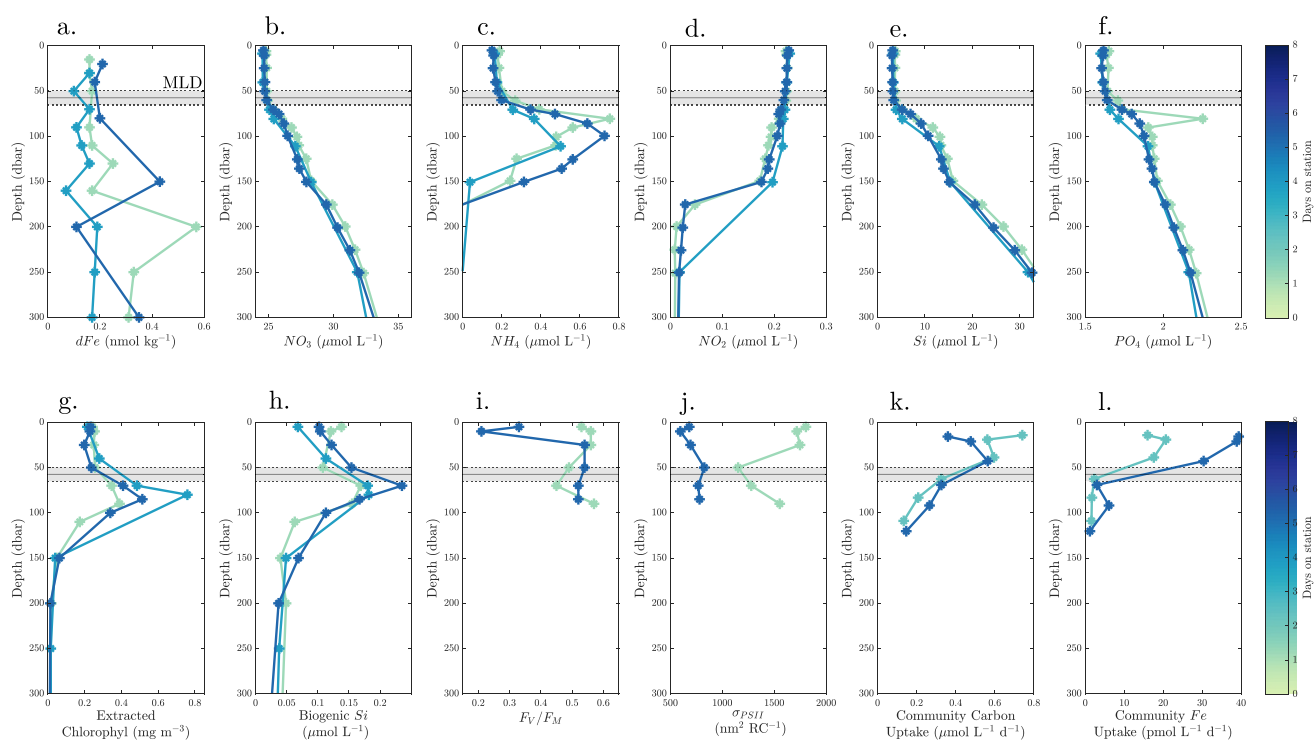


Figure 2. Vertical profiles for the 56°S station from CTD rosette water samples. Dissolved Fe samples were sampled from a trace metal clean rosette. (a) Dissolved Fe (dFe), (b) nitrate, (c) ammonium, (d) nitrite, (e) silicate, (f) phosphate, (g) extracted Chl, (h) biogenic silica, (i) F_v/F_m , (j) σ_{PSII} , (k) community carbon fixation and (l) community iron uptake. MLD and color bar are as for Figure 1.

subsurface feature was observed at the base of the seasonal thermocline in the zone where both nitrate (from 25 to $\sim 28 \mu\text{mol L}^{-1}$) and silicate (from 4 to $>10 \mu\text{mol L}^{-1}$) concentrations increased with depth (Figures 2b and 2e). However, the DCM was not co-located with the ferricline ($\sim 0.2 \text{ nmol kg}^{-1}$ dissolved Fe (dFe) in the DCM cf. $>0.4 \text{ nmol kg}^{-1}$ at depth, Figure 2a). The DCM/DBM feature coincided with a subsurface ammonium maximum in all profiles where ammonium was sampled (Figure 2c). The Tmin layer, a relict feature from winter water, is often associated with a subsurface ammonium maximum that is present during winter in the IPFZ (Mdutyana et al., 2020). Hence, it was assumed that the subsurface ammonium maximum was also present over winter at the 56°S (and 58°S) site within the IPFZ.

Discrete samples from the CTD rosette were analyzed for biological metrics such as BSi (Figure 2h), F_v/F_m (Figure 2i), and NPP and Fe uptake rates (Figures 2k and 2l). Extracted chlorophyll measurements confirmed the presence of a DCM ($>0.7 \text{ mg m}^{-3}$ cf. 0.2 mg m^{-3} within the mixed layer, Figure 2g). At the 56°S site, BSi was measured at $\sim 0.1 \mu\text{mol L}^{-1}$ in the mixed layer but increased to $0.2 \mu\text{mol L}^{-1}$ within the DCM—indicative of a diatom-dominated subsurface feature (Figure 2h). Si^* —a proxy for diatom iron stress (Brzezinski et al., 2002)—was $\sim 20 \mu\text{mol L}^{-1}$ in the surface mixed layer and constant over the site occupation (Figure S5 in Supporting Information S1). The DCM/DBM was collocated with a deep particulate phosphorus (P) maximum (80 nmol kg^{-1} cf. $\sim 30 \text{ nmol kg}^{-1}$ in the mixed layer, (Figure S6 in Supporting Information S1, $>99.9\%$ confidence, see Supporting Information S1) but was only associated with a small increase in particulate Fe stocks (0.1 nmol kg^{-1} in the DCM, cf. $<0.1 \text{ nmol kg}^{-1}$ in the mixed layer, Figure S6 in Supporting Information S1).

Light microscopy revealed that the DCM/DBM was dominated by large diatoms comprising many species (Figure S7 in Supporting Information S1). Cells in the subsurface feature had an F_v/F_m of ~ 0.5 , whereas those in the mixed layer had either equivalent or lower values (Figure 2i). The functional absorption cross section of PSII (σ_{PSII}) was variable and ranged from 600 to $1,500 \text{ nm}^2 \text{ RC}^{-1}$ across two profiles (Figure 2j). Carbon (i.e., NPP) and Fe (by phytoplankton and heterotrophic bacteria) uptake profiles (Figures 2k and 2l) exhibited significantly low iron uptake rates within the DCM/DBM ($\sim 2 \text{ pmol L}^{-1} \text{ d}^{-1}$, cf. up to $40 \text{ pmol L}^{-1} \text{ d}^{-1}$ in the mixed layer, $>99.9\%$ confidence, see Supporting Information S1) with large cells contributing $\sim 60\%$ to the community

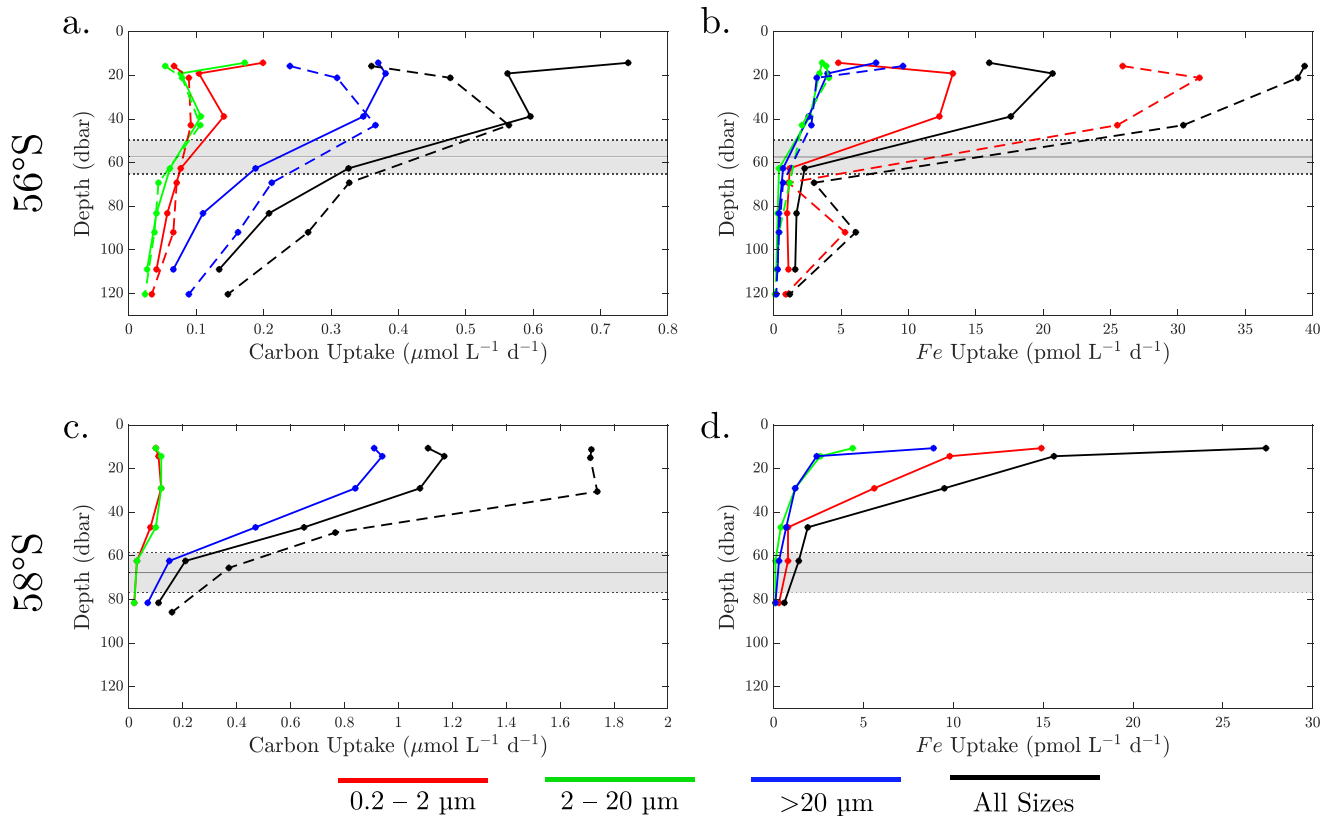


Figure 3. Size-partitioned C and Fe uptake rates for three size classes and their sum (all sizes) at 56°S (solid lines 20 December 2020; dashed lines 26 December 2020) and 58°S (solid lines 29 December 2020, dashed lines 7 January 2021).

integrated NPP rate at depth (Figure 3). In contrast, NPP was $\sim 0.3 \mu\text{mol L}^{-1} \text{d}^{-1}$ within the DCM/DBM (cf. $0.7\text{--}0.8 \mu\text{mol L}^{-1} \text{d}^{-1}$ in the mixed layer, Figure 2k). Large cells ($>20 \mu\text{m}$) dominated C uptake in both the mixed layer and DCM (Figure 3), resulting in low Fe:C uptake ratios ($3.3\text{--}4.5 \mu\text{mol}:\text{mol}$), indicative of cells in steady-state. The dominant zooplankton were salps (*Salpa thompsoni* with comparable abundances, collected using a $335 \mu\text{m}$ mesh neuston net) during the day ($1.207 \pm 0.441 \text{ ind. } 10 \text{ m}^{-3}$) than during the night ($0.908 \pm 0.301 \text{ ind. } 10 \text{ m}^{-3}$) in the upper 200 m of the water column.

In contrast, at the 58°S site there was no evidence of a DCM and DBM until almost the end of our site occupation (Figures 4d and 4e), with relatively high chlorophyll stocks (0.6 mg m^{-3} (extracted value) within the seasonal mixed layer (Figure 5g and Figure S8 in Supporting Information S1). From a physical perspective, ship-based sampling revealed that the water column had a colder ($1\text{--}1.2^\circ\text{C}$) and deeper (225–275 m depth, Figure 4a) T_{min} feature than at the 56°S site ($1.75\text{--}2.0^\circ\text{C}$ and $\sim 200 \text{ m}$ depth, Figure 2a). Importantly, both features overlie a 2.5°C layer of Upper Circumpolar Deep Water (UCDW), suggesting similar winter water mass initial composition (Figure S6 in Supporting Information S1). Biogeochemically, detrital POC made up a smaller proportion (~ 0.8) in the surface mixed layer at 58°S (Figure 4g) relative to the 56°S site (Figure 1g). At the 56°S site, a subsurface ammonium maximum was evident below the mixed layer (Figure 5c) and coincided with the upper stratum of the T_{min} layer (Figure 5a). At the 58°S site, BSi was $0.2\text{--}0.3 \mu\text{mol L}^{-1}$ within the surface mixed layer (Figure 5h) and Si^* in the mixed layer was significantly lower ($\sim 25 \mu\text{mol L}^{-1}$) than at the 56°S site and decreased during our site occupation (Figure S5 in Supporting Information S1, $>99.9\%$ confidence, see Supporting Information S1). Particulate P was $80\text{--}120 \text{ nmol kg}^{-1}$ in the mixed layer (Figure S6 in Supporting Information S1) and particulate Fe was variable with depth ($0.1\text{--}0.4 \text{ nmol kg}^{-1}$, Figure S6 in Supporting Information S1). Phytoplankton cells exhibited F_v/F_m of ~ 0.45 in the surface mixed layer (Figure 5i) and a σ_{PSII} of $>800 \text{ nm}^2 \text{RC}^{-1}$ (Figure 5j) in this stratum. NPP rates were significantly higher than those at the 56°S site (Figures 3a and 3b, Table S1 in Supporting Information S1, $>99.9\%$ confidence, see Supporting Information S1), but community Fe uptake rates were comparable (Figures 3c and 3d). As observed for the 56°S site, cells $<2 \mu\text{m}$ dominated Fe

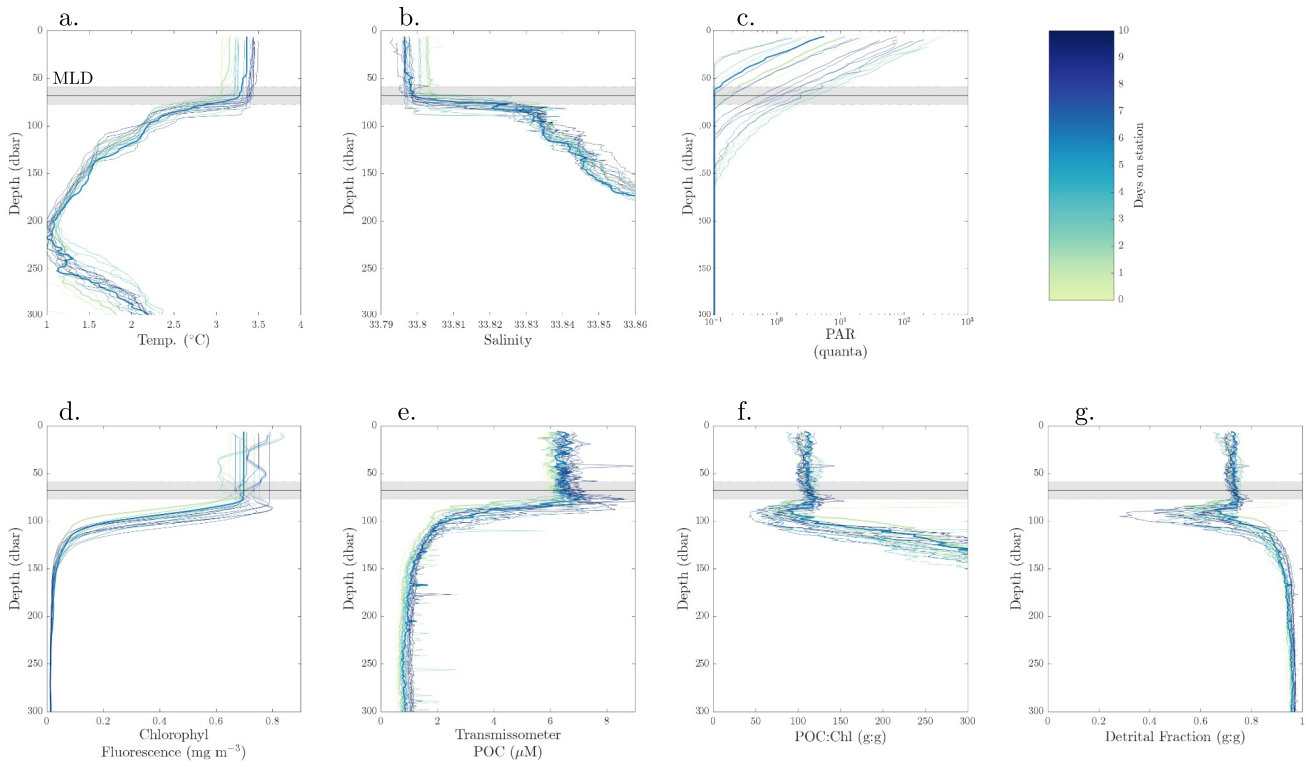


Figure 4. Vertical profiles for the 58°S station from calibrated CTD sensors. Panels are as for Figure 1, as are the MLD definition and the color bar. Arrival on station (day 0) was 1 January 2021. Note that no DCM or DBM was located using our algorithm (see Methods) at 58°S. Chlorophyll profiles with uniform surface values in the euphotic zone were obtained during day-casts and have been NPQ corrected.

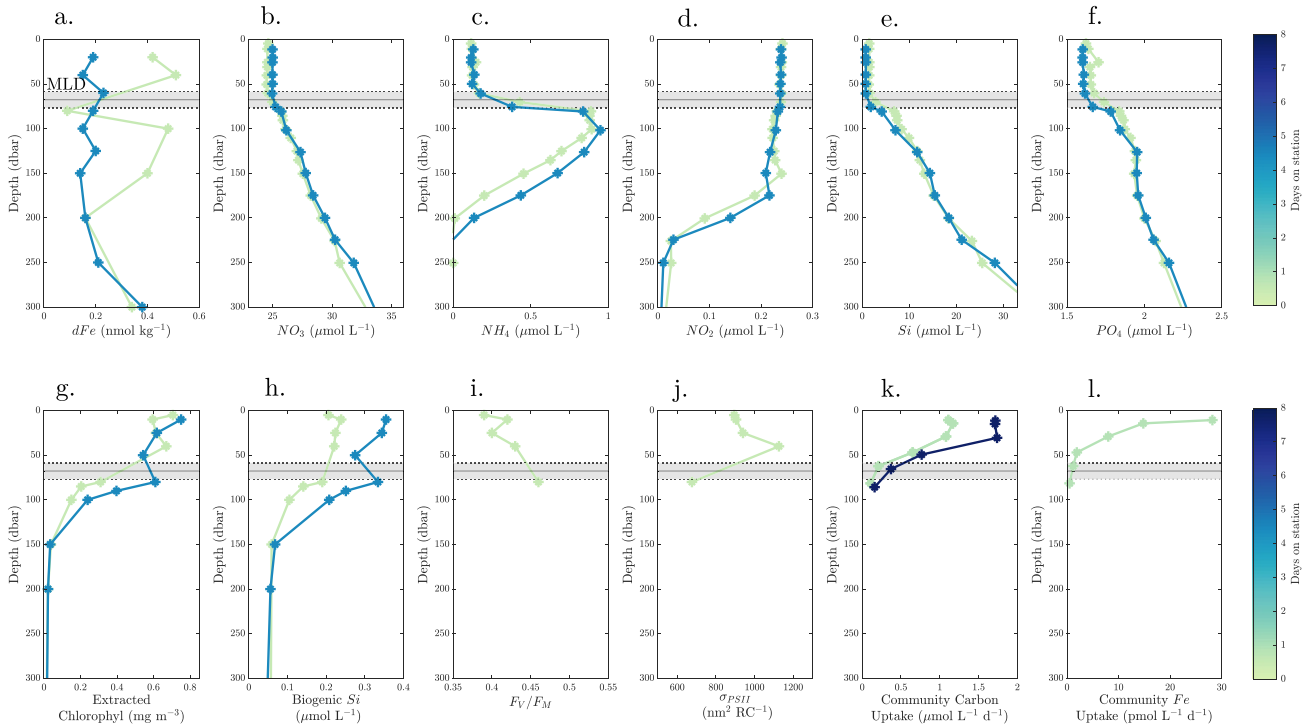


Figure 5. Vertical profiles for the 58°S station from CTD rosette water samples. Dissolved Fe samples were sampled from a trace metal clean rosette. Panels are as for Figure 2 and MLD and color bar are as for Figure 3.

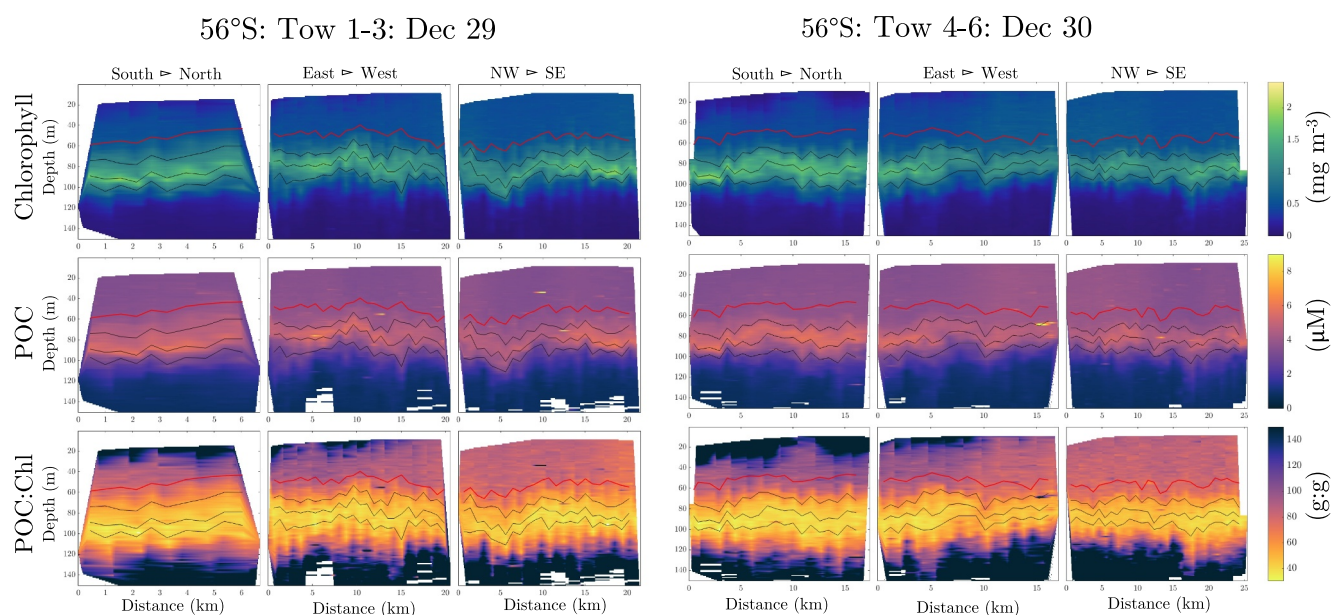


Figure 6. Triaxus towbody sections in the vicinity of the 56°S station (see Figure S2 in Supporting Information S1 for towbody maps that relate to the direction of the tow presented above the panels for Chlorophyll) for Chlorophyll, POC and C:Chl ratio. The red vertical line in each panel denotes the mixed layer depth. The DCM and DBM peak (i.e., maximum concentration) and vertical extent are calculated as per Figure 1 for each profile of the towbody and denoted with black lines.

uptake, while cells $>20 \mu\text{m}$ dominated NPP (Figure 3). Salps also dominated the zooplankton community, and abundances (0–200 m depth) were comparable to those at 56°S and similar at night ($0.582 \pm 0.387 \text{ ind. } 10 \text{ m}^{-3}$) than during the day ($0.388 \pm 0.254 \text{ ind. } 10 \text{ m}^{-3}$). Note, that at both sites, the variability between net tows was high due to a patchy salp distribution, as reflected in the large standard deviations.

3.2. Spatial and Temporal Patterns in the DCM Feature Around 56°S and 58°S

The spatial extent of the DCM/DBM and the relationship with environmental drivers of this feature around the two sites were explored using Triaxus towbody surveys of around 48–64 km comprising three sections at each site (Figure S2c in Supporting Information S1 and Figures 6 and 7). An initial Triaxus tow of $\sim 56 \text{ km}$ (55.75°S 138.65°E to 138.3°E , Figure S2 in Supporting Information S1) to the west of the site under darkness (to avoid NPQ) exhibited constancy in both the IPFZ water mass characteristics and the location of the DCM (Figure 6). Towbody observations also revealed the presence of a coincident DBM of $\sim 20 \text{ m}$ thickness located at 80 to $>100 \text{ m}$ depth. The POC:Chlorophyll ratios (note POC will contain non-phytoplankton cells) were typically lower (~ 40) within the DCM/DBM than in the overlying mixed layer (~ 80) reflecting the greater contribution of chlorophyll to this feature relative to POC (Figure 6 cf. 1f).

Several additional tows at the 56°S site further corroborated that the DCM was a more widespread feature beyond our study site (Figure 6). However, there was some spatial variability along each leg of the Triaxus tows in both the depth, thickness and magnitude of the DCM. The relationship with the depth and thickness of the DCM relative to that of the DBM provides clues as to the environmental forcing of this feature on short temporal and spatial scales. The depth of the DCM and DBM was well correlated and generally co-located (within $\sim 5 \text{ m}$) during all tows that identified both a DCM and DBM. However, the DCM was consistently slightly deeper ($\sim 5 \text{ m}$) than the DBM, suggesting the increasing role of photoacclimation with depth. The thickness of the DCM and DBM were also well correlated, with the DCM typically $\sim 5 \text{ m}$ thicker than the DBM. The absolute magnitude of the DCM and DBM were generally well correlated; however, the deep enhancement of the DCM was greater than that of the DBM (see Figure 6).

At the 58°S site, there was evidence of temporal evolution of a co-located DCM and DBM near the study site. This emerging feature is most conspicuous on 11 January, 2021 on tow 3/5 (i.e., the S-N return leg to the 58°S study site (Figure 7 and Figure S1 in Supporting Information S1). During the first towbody deployment at 58°S, the DCM thickness was much more variable than that of the DBM (Figure 7). A comparison of the features at both

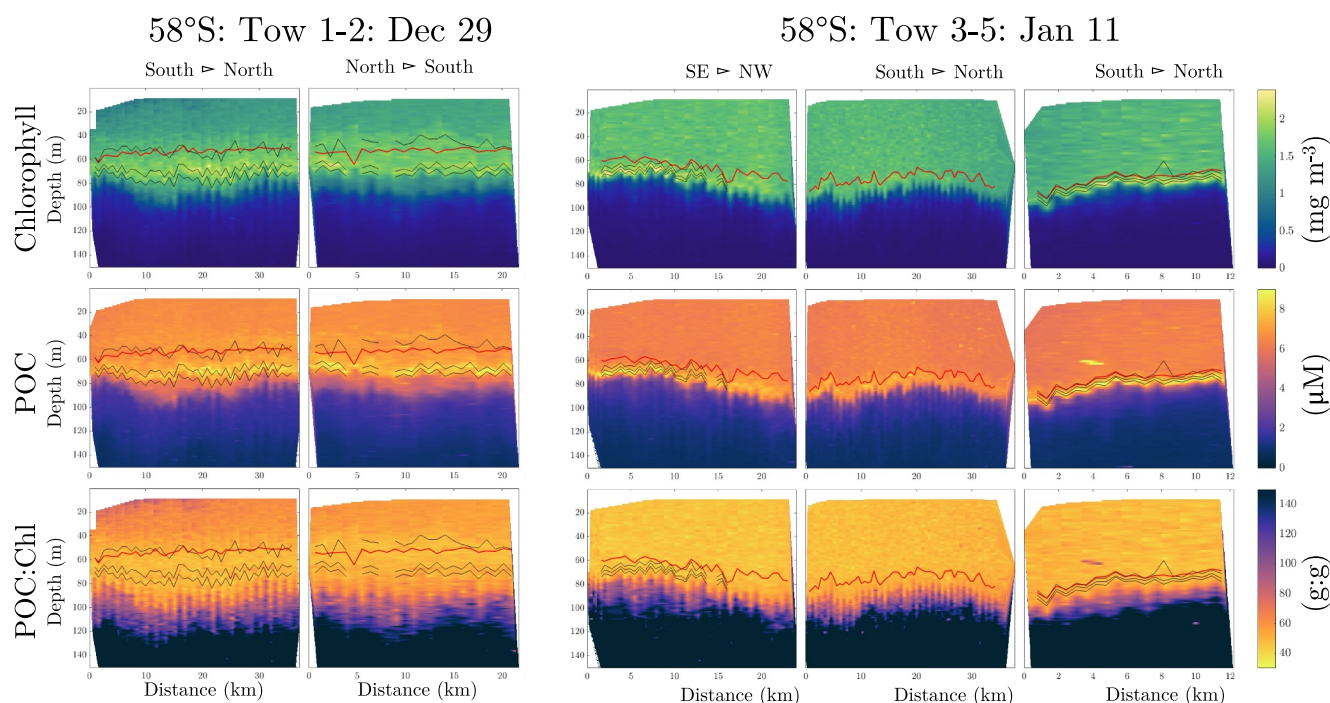


Figure 7. Triaxus towbody sections in the vicinity of the 58°S station. As per Figure 6. Note that discontinuities in the DCM/DBM time-series indicate no DCM/DBM was located using our algorithm for that leg of the tow.

sites revealed that the absolute magnitudes of the DCM and DBM were larger at 58°S than 56°S, whereas the deep enhancement of the DCM and DBM was substantially larger at 56°S compared to 58°S (Figure S4 in Supporting Information S1). At 56°S chlorophyll was enhanced by >1–4 fold across the DCM relative to the surface mixed layer, coincident with a smaller but substantial 20%–60% enhancement of POC. In contrast, at 58°S, deep enhancement of chlorophyll and C did not exceed ~25% in any profile.

The seasonality and downward export potential of the DCM observed in the IPFZ at the 56°S site were explored using the BGC-ARGO float. The float data sets extended the week-long shipboard observations for 3–4 months within the IPFZ water mass (Figure S2a in Supporting Information S1) and thus can be cautiously linked to shipboard trends presented in Figures 1, 2, and 5. The float’s multi-sensor constellation provides insights into the temporal evolution of physical (Figure 8) and bio-optical (Figure 9) properties over the ensuing months from austral summer into autumn/fall 2021, allowing us to track changes in the characteristics of the DCM/DBM (thickness, POC:Chlorophyll, depth) and its environment. The distinctive DCM/DBM feature we observed from the CTD profiles (Figure 1) and the Triaxus tow-body (Figure 7) was also evident from the BGC-ARGO float observations for ~3 additional months. The joint presence of the DCM and DBM spanned late December 2020 to late March 2021 (Figures 9a and 9b) and exhibited a comparable gradient in C:Chlorophyll ratios, which decreased with depth (Figures 9c and 9d) as observed with the towbody (Figure 6). There was no marked change in the POC:Chlorophyll ratio in the DCM over several months (Figure 9c), which we interpret as indicative of a persistent healthy population of large diatoms, based on the float profiles obtained during our shipboard occupation of this site.

The magnitude (~0.6 $\mu\text{g L}^{-1}$, Figure 2g, cf. Figures 1d and 1a, depth (80–100 m) and thickness (20–25 m) of the subsurface feature were largely consistent for 3 months (Figure 9) despite pronounced changes in the depth of the surface mixed layer, which varied from <50 to ~100 m depth (Figure 8). The DCM/DBM decreased in amplitude and thickness in late March, which coincided with a programmed change in the sampling frequency of the float from 2 to 5 days (for several profiles) and followed by a shift to 10-day intervals (i.e., ARGO standard protocol). The cause of the demise of the DCM/DBM feature is unclear but may be linked to the threefold seasonal decrease in incident irradiance in April 2021 that is reflected in underwater PAR of <2 $\mu\text{mol quanta m}^{-2} \text{s}^{-1}$ within the subsurface feature (Figure S9 in Supporting Information S1).

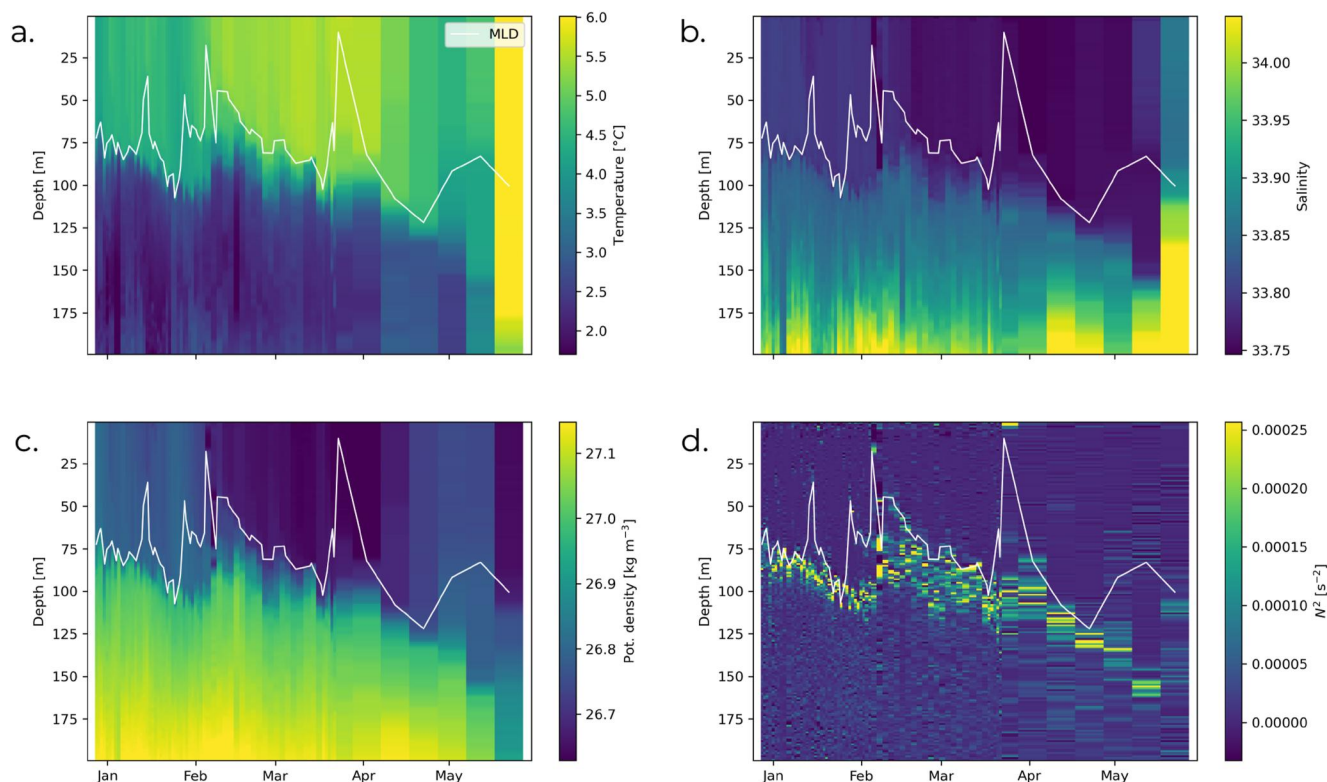


Figure 8. Time-series of BGC-ARGO physical observations (semi-log plots) in the vicinity of the 56°S site. (a) Temperature, (b) salinity, (c) potential density, and (d) Brunt-Väisälä frequency (i.e., buoyancy frequency). MLD denotes the seasonal mixed layer depth (white line).

The fate of the large diatoms within this feature is also unclear. There was no evidence of a distinct downward particle pulse in either the BCG-ARGO chlorophyll or POC time-series associated with the decline of the DCM/DBM feature (Figure 10). However, there is some evidence of a small but constant flux of particles from January to March 2021 from the backscatter sensor on the float (Figure 10b) that is less conspicuous in the float fluorometer time-series (Figure 10a). This observation suggests that the diatoms residing within the subsurface features may have sunk to depth intact as both cells and empty frustules.

4. Discussion

The different observational modes we employed to study the DCM/DBM feature within the IPFZ along with the diverse range of metrics from biogeochemical to photo-physiological, enable us to probe many facets of this polar subsurface feature. We explore the timing of DCM/DBM formation at each site relative to the seasonal productivity cycle of the overlying waters. Next, we consider potential drivers for the DCM formation and then compare and contrast its characteristics with the biogeochemical fluxes we measured. We further interpret towbody and BGC-ARGO observations to examine its wider-scale spatial and temporal distribution. The floating data also enable us to address questions about its longevity and fate. Together, these multiple lines of examination provide insights into the DCM's ecological and biogeochemical roles in the S. Ocean.

4.1. Timing of DCM/DBM Formation

Here, we attempt to constrain the formation of the DCM/DBM features observed at the 56°S and 58°S sites (Figure 1 cf. Figure 4) by placing them in the context of the seasonal productivity cycle within the IPFZ region using a time-series of satellite ocean color (Figure S10 in Supporting Information S1). This enables exploration of whether the DCM/DBMs that formed at each site took place when mixed layer chlorophyll was increasing or declining seasonally. The onset of increases in surface mixed layer chlorophyll (i.e., based on exceeding an arbitrarily assigned threshold of 0.4 μg chlorophyll L^{-1} (the upper limit of canonical values in iron-limited HNLC waters, Boyd & Abraham, 2001) are evident from the ocean color composite images for November 13 and 21

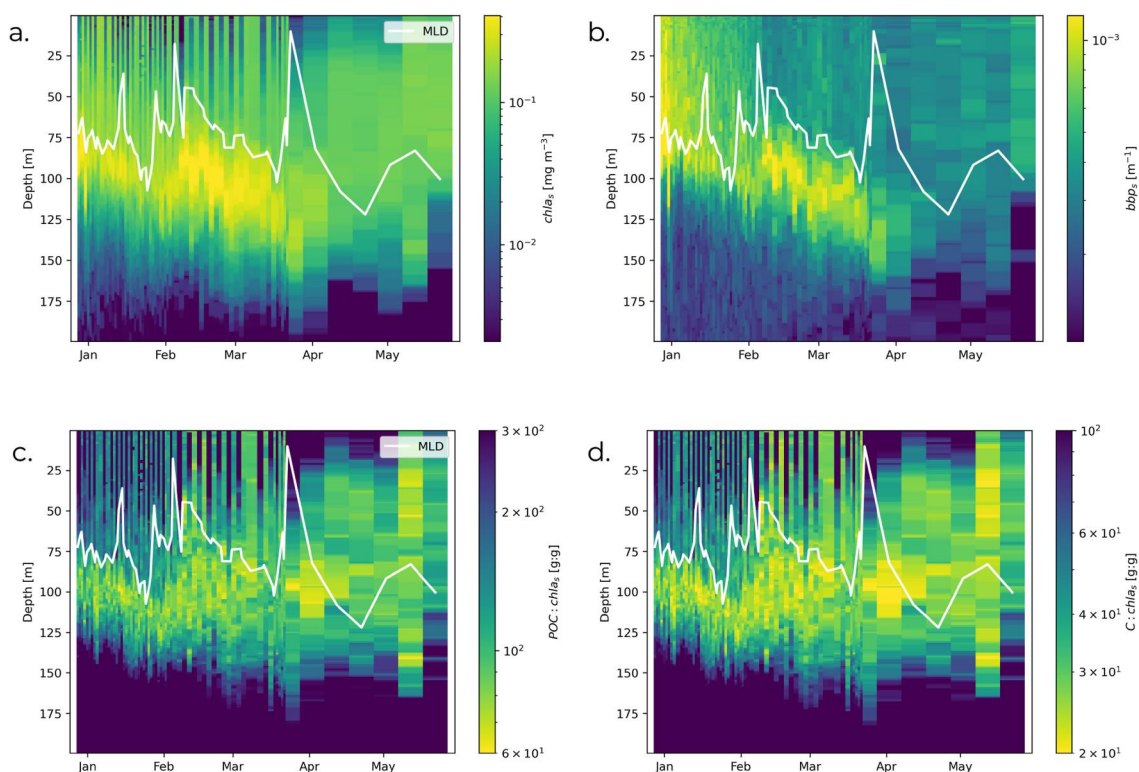


Figure 9. Time-series of BGC-ARGO biological observations (semi-log plots) in the vicinity of the 56°S site. (a) Concentration of small fluorescing particles chl_{a_s} and (b) small backscattering particles bbp_s , (c) POC: chl_{a_s} ratio and (d) algal C: chl_{a_s} ratio (see Methods). MLD denotes the seasonal mixed layer depth (white line).

2020 at the 56°S and 58°S sites, respectively (Figures S10 and S11 in Supporting Information S1). Conspicuous decreases in chlorophyll stocks (i.e., $<0.4\ \mu g$ chlorophyll L^{-1}) are observed from the composites for 15 December 2020 at the 56°S site but not until 16 January 2021 at the 58°S site (Figures S10 and S11 in Supporting Information S1).

At the 56°S site, we observed a well-established (i.e., it did not evolve further during our time on stations, Figure 1) DCM/DBM feature during late December, about 10 days after satellite observations revealed chlorophyll stocks declining in the surface mixed layer. This feature also exhibited a deep minimum in the POC/Chlorophyll ratio (Figures 1 and 6), suggesting the joint contribution of biomass and photoadaptation to the DCM. At the 58°S site, we observed the simultaneous onset of a DCM and DBM feature around 10 January 2021 (Figure 5 and Figure S8 in Supporting Information S1), when chlorophyll was $0.59\ \mu g\ L^{-1}$ in the mixed layer (Table S1 in Supporting Information S1), around a week before there was a conspicuous decrease in mixed layer

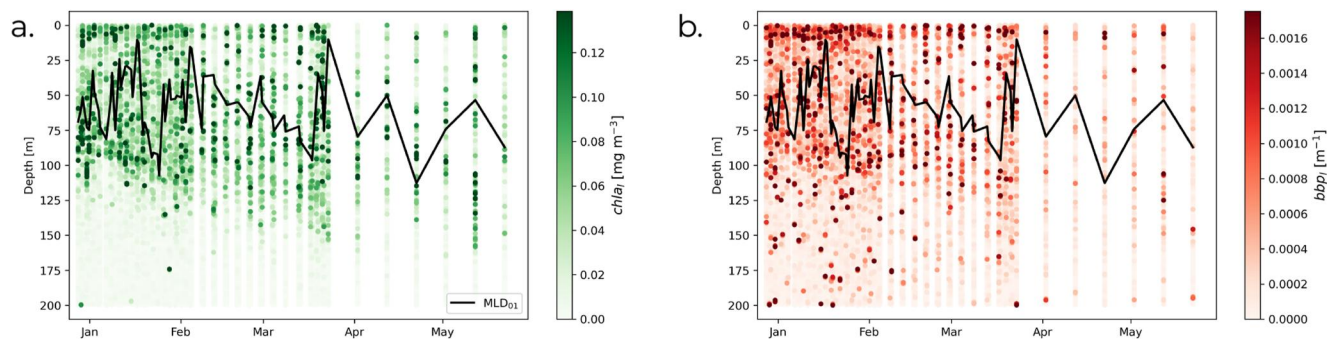


Figure 10. Time-series of BGC-ARGO biological observations in the vicinity of the 56°S site presented in Figures 9a and 9b, but replotted with a linear (rather than log) colormap to better assess the potential export of Chl and C into the oceans' interior. (a) Concentration of large fluorescing particles chl_{l1} . And (b) large backscattering particles bbp_{l1} . The black line denotes the seasonal mixed layer depth.

chlorophyll stocks based upon the satellite composites (Figures S10 and S11 in Supporting Information S1). Here, there was less evidence of photoadaptation in the emerging feature (i.e., a less pronounced minimum in the POC: Chlorophyll ratio, Figures 4 and 7).

A prior study (Parslow et al., 2001) recorded an earlier springtime DCM at 53°S (i.e., near the northern edge of the IPFZ) during November 1995. Parslow et al. (2001) reported a diatom-dominated feature at ~65 m depth that was not present in a prior October 1991 transect in the IPFZ. They reported data on chlorophyll ($0.7 \mu\text{g L}^{-1}$ cf. $0.3 \mu\text{g L}^{-1}$ in the overlying surface mixed layer) and pigments but not for backscatter or transmissivity; therefore, it is not known if there was also a DBM in the November 1995 feature. However, they did present values of alpha (the slope of the phytoplankton photosynthesis-irradiance curve) that were two-fold higher in the DCM phytoplankton community compared to overlying waters, suggesting a low light-acclimated phytoplankton population, and hence potentially no DBM.

Generalizing across (a) an established DCM feature with strong evidence of photoadaptation observed at 53°S in November (Parslow et al., 2001); (b) an established DCM/DBM feature with evidence of photoadaptation contributing to the magnitude of the DCM observed at 56°S in late December, 10 days after mixed layer chlorophyll stocks began to decline; and (c) the concurrent emergence of a DCM and DBM with little contribution of photoadaptation observed at 58°S in early January, a week prior to the seasonal decline of surface chlorophyll, we can begin to infer the seasonal distribution of DCM formation across the IPFZ. All three lines of evidence are consistent with a north-to-south progression in the formation of a DCM/DBM feature across the IPFZ following a north-to-south progression of seasonal surface productivity observed by satellite (Figure S10 in Supporting Information S1). This subsurface feature appears to begin to emerge concurrently as a DCM and DBM 7–10 days before surface chlorophyll stocks decline and then persist after surface chlorophyll is depleted.

4.2. Drivers of DCM/DBM Formation

Here, we explore the evidence for factors, such as resource limitation, leading to the formation of a DCM/DBM (see Lande et al., 1989). In contrast to the 53°S feature studied in November 1995 by Parslow et al. (2001), silicate concentrations were low and vanishingly low in the surface mixed layer of our more southern polar sites at 56°S and 58°S, respectively (Figures 2 and 5). Parslow et al. (2001) also reported low silicate concentrations (along with DFe of 0.2 nmol kg^{-1}) in DCMs near 54°S (i.e., within the IPFZ) in January over several different years. At both our sites, DFe was $\sim 0.2 \text{ nmol kg}^{-1}$ (Figures 2 and 5), suggesting Fe stress, based on the relationship between DFe concentration and F_v/F_m reported for the polar S. Ocean in Boyd and Abraham (2001). Si*—another proxy for Fe stress—was $\sim 20 \mu\text{mol L}^{-1}$ at both sites, and decreased further during the site occupation at 58°S, also suggesting increasing phytoplankton physiological stress (Figure S5 in Supporting Information S1). Furthermore, at the 56°S and 58°S sites, chlorophyll (and NPP) in the mixed layer were 0.3 mg m^{-3} ($\sim 600 \text{ mg C m}^{-2} \text{ d}^{-1}$) and 0.6 mg m^{-3} ($\sim 1,000 \text{ mg C m}^{-2} \text{ d}^{-1}$) (Figures 2 and 5), respectively, supporting the conclusion from the ocean color remote-sensing (Figure S10 in Supporting Information S1) that surface mixed layer at the 56°S site at the time of occupation was at a later, declining, stage of development in its seasonal primary productivity cycle.

At the 58°S site, based on drawdown in silicate between the two profiles (obtained while tracking a holey sock drogue, and so quasi-Lagrangian), 4 days apart (Figure 5h), the demand for silicate is $0.176 \mu\text{mol L}^{-1} \text{ d}^{-1}$, which is ~ 5 -fold lower than the rate measured for the Pacific sector of the S. Ocean, $\sim 1 \mu\text{mol L}^{-1} \text{ d}^{-1}$ (Sigmon et al., 2002) at a similar latitude. This, along with low and decreasing silicate stocks, suggests that cells at this site are close to Si limitation. Thus, it is likely that the 58°S site would be on the verge of transitioning to a decline in phytoplankton stocks (Figures S10 and S11 in Supporting Information S1) and NPP driven by silicate and/or Fe limitation. These conditions may have led to the development of a DCM/DBM (see DCM/DBM in S-N tow on 11 January 2021 in Figure 7 and CTD profiles in Figure S8 in Supporting Information S1) around 10 January 2021 (i.e., toward the end of our ship-based observational record at the 58°S site).

How did the subsurface feature develop and where was it initiated within the water column? The gradual enhancement of the subsurface features evident in Figure S8 in Supporting Information S1, assuming it was in the same water mass (Figure S12 in Supporting Information S1), suggest that a DCM and DBM evolved at depth at a time when there is chlorophyll $>0.4 \mu\text{g L}^{-1}$ in overlying waters and a correspondingly high light attenuation coefficient. Therefore, this suggests the hypothesis put forward by Cornec, Claustre, et al. (2021) on DCM formation—in which there is in situ enhancement of the DCM/DBM driven by reduced light attenuation at depth due to the decline of the stocks in the mixed layer—does not fit this S. Ocean scenario. Furthermore, in the surface

mixed layer, the estimated phytoplankton turnover times based on POC stocks and NPP (Table S1 in Supporting Information S1) are higher than in the DCM, despite the onset of Fe and/or Si limitation. This suggests that the build-up of the subsurface feature must require low loss terms, in particular low loss rates due to herbivory. The resident large diatoms present at the 56°S site have highly silicified frustules (Figure S7 in Supporting Information S1) thought to be an evolutionary mechanism to prevent/minimize grazing (Smetacek, 2001) and are evident in their ability to resist salp herbivory (Figure S13 in Supporting Information S1). Thus, a combination of bottom-up (onset of silicate and/or Fe limitation in the surface mixed layer) and top-down (low loss terms to grazers) may lead to the onset of DCM/DBM formation, but whether this formation takes place at depth or originates within the mixed layer via the relocation of a subset of the phytoplankton population (the large diatoms) via slow sinking/buoyancy regulation remains an open question.

In the next section, we explore key physiological characteristics of the subsurface feature observed at the 56°S and 58°S sites, such as phytoplankton species composition and Fe uptake rates, to further explore the drivers that led to DCM/DBM formation.

4.3. DCM/DBM Characteristics and Biogeochemical Fluxes

The feature at 56°S had several distinctive characteristics that enabled us to further probe the validity of silicate and/or Fe limitation as key environmental triggers in the initiation of a DCM. The subsurface phytoplankton assemblage differed from that in the overlying water column (Figure S7 in Supporting Information S1). Based on light microscopy, the DCM/DBM was dominated by large diatoms, many >200 μm in length, comprising multiple species (see Figure S7 in Supporting Information S1). Multiple diatom species have also been recorded in a DCM in the Indian sector of the S. Ocean by Gomi et al. (2010). At our 56°S site, observations from microscopy are supported by a >3-fold higher BSi concentration in the DCM relative to the overlying mixed layer (Figure 2h). Size-fractionated NPP and Fe uptake revealed that the large cells (>20 μm fraction) dominated NPP within the DCM ($0.1 \mu\text{mol L}^{-1} \text{d}^{-1}$) (Figure 3), had a relatively high photosynthetic competence (F_v/F_m , Figure 2i cf. theoretical maximum of 0.65 see Boyd & Abraham, 2001), and very low Fe requirements at 56°S (Figure 3b). These low Fe requirements for large polar diatoms are also observed in lab cultures (using some of the species observed in the DCM/DBM) and are attributed to the cells' ability to increase the size of their light-harvesting antenna under low light conditions (with implications for self-shading, see later) rather than increase the number of photosystem units in the chloroplast, which has an added Fe cost for effective light harvesting under low irradiances (Strzpek et al., 2012). Irradiances at the base of the DCM were low during the daytime ($1\text{--}20 \mu\text{mol photons m}^{-2} \text{s}^{-1}$, Figure 1c and Figure S9b in Supporting Information S1), suggesting that large polar diatoms may be particularly well suited to persist in the poorly lit DCM/DBM relative to other species with higher iron requirements at such low irradiances.

The findings of a shipboard perturbation experiment conducted at the 56°S site in which dFe, manganese and irradiance were amended either alone or in combination (Latour et al., 2023) reveal some evidence of Fe limitation of the resident cells within the DCM/DBM. Although some of the treatments, such as increasing both Fe and irradiance, do not reflect conditions within the overlying mixed layer at 56°S, these perturbations do provide valuable insights into the physiological status of the cells within the DCM/DBM. Latour et al. (2023) reported that the transfer of resident cells to more optimal conditions (high irradiance and high Fe) led to a major upregulation in their physiology, as evidenced by marked increases in chlorophyll, POC and BSi stocks (relative to a high light only treatment). Thus, diatoms probably exist in the DCM/DBM with sufficient resources for low rates of NPP (Figure 3) in a subsurface niche that enables them to continue to be productive for months. However, the perturbation experiments by Latour et al. (2023) strongly suggest that these cells remain primed for more optimal conditions (such as nutrient replete and high light, where they could grow faster (Table S1 in Supporting Information S1)), as observed in high-latitude polar regions of the Arctic (Hoppe, 2021) and Antarctic (Kennedy et al., 2019).

Other characteristics of the 56°S site provide insights into what might lead to the initiation of a DCM/DBM as a niche for large diatoms. The ferricline at the 56°S site was >100 m deeper than the seasonal mixed layer (Figure 1a cf. 2a), indicating that the observed persistence of the DCM/DBM for months (Figure 9) likely requires another source of Fe, since the $\sim 4 \text{ pmol L}^{-1} \text{d}^{-1}$ Fe demand by large cells would lead to a cumulative demand of $>0.1 \text{ nmol L}^{-1} \text{month}^{-1}$ (assuming this observed Fe uptake rate (Figure 3b) was applicable beyond our site occupation in late December 2020). Where could this Fe be supplied from? It is unlikely that episodic resupply by

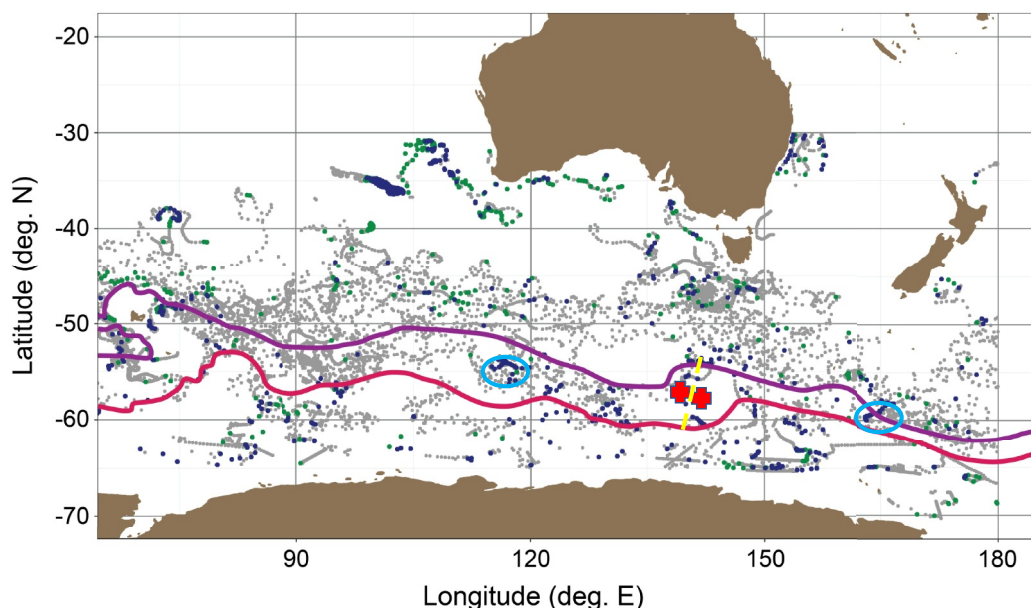


Figure 11. Indo-Pacific sectors of the S. Ocean overlaid with composite of the locations of BGC-ARGO float profiles presented in Cornec, Claustre, et al. (2021). Blue small symbols denote float profiles where DCM and DBMs were observed. Green symbols represent where only DCMs (but no DBM) were recorded. Gray symbols represent where no DCMs were observed. Two floats that recorded persistent DCM features are highlighted with light blue circles at 120°E and 165°E. The two polar sites (56°S 138.5°E, 58°S 141.5°E) featured in our study are denoted by red crosses. The SR3 line (from Tasmania to E. Antarctica) along which Parslow et al. (2001) recorded DCMs only within the IPFZ over multiple years during WOCE and JGOFS transects is represented by a yellow dashed line. The purple and red lines denote the fronts which bound the IPFZ.

storm-driven mixing (Du Plessis et al., 2022) down to the depth of the ferricline occurred as it would have eroded the T_{min} layer. Such erosion was not evident from vertical profiles obtained from BGC-ARGO (Figure 8). Also, although salp fecal pellets are a major source of recycled iron (Böckmann et al., 2021), the salp distribution was patchy and unlikely to be able to provide sustained iron supply for 3 months during which the DCM/DBM persisted. Subsurface ammonium maxima reflect the signature of microbial remineralization in many locales including the S. Ocean (see Mduyana et al., 2020). So, is it possible that the co-location of the DCM/DBM with the upper zone of the subsurface ammonium maximum (Figure 2) indicates a role in for a recycled Fe iron supply to the diatoms within the DCM/DBM?

Prior measurements of ammonium and dFe recycling made during an in situ particle remineralization study at 180 m depth in a subantarctic site revealed that 0.78 nmol L⁻¹ dFe was released per 0.38 μmol L⁻¹ of ammonium produced, equating to a resupply ratio of 2.06 nmol L⁻¹ dFe per μmol L⁻¹ of ammonium released (Bressac, unpublished). The subsurface ammonium maximum was ~0.6 μmol L⁻¹ at the 56°S (Figure 2c) and approximates steady-state based on three profiles within 9 days. Assuming a conservative turnover time of 100 days for the subsurface ammonium maximum (cf. Mduyana et al., 2020), this feature could potentially release ~12 pmol dFe L⁻¹ d⁻¹, more than meeting the measured diatom Fe requirements (Figure 3b). The subsurface ammonium feature that characterizes the T_{min} layer (Figures 2c and 5c) is present over winter when it is already dynamic, as reported for the IPFZ in the Atlantic sector by Mduyana et al. (2020). In other systems, Fe recycling within the DCM/DBM is reported to play a key role, for example, in sustaining the diatom-dominated feature in the Mediterranean Sea (Marañón et al., 2021).

Another candidate mechanism for DCM/DBM formation is the alleviation of diatom silicate limitation, as silicate was at low and vanishingly low levels at the 56°S and 58°S sites, respectively, and the DCM was co-located with a subsurface peak in BSi (Figures 2e, 2h and Figures 5e, 5h). At 90 m depth, the base of the DCM at 56°S, silicate was present at ~10 μmol L⁻¹ (Figure 2e). As the DCM persisted for months after our site occupation (Figure 9), a continuing source of silicate is likely required for this feature's ongoing presence. S. Ocean diatoms have been reported to have a low affinity for silicate, especially south of the Polar Front. For example, Nelson et al. (2001) reported half-saturation constants of >10 μmol L⁻¹ for some species north of the Ross Sea during the AESOPS

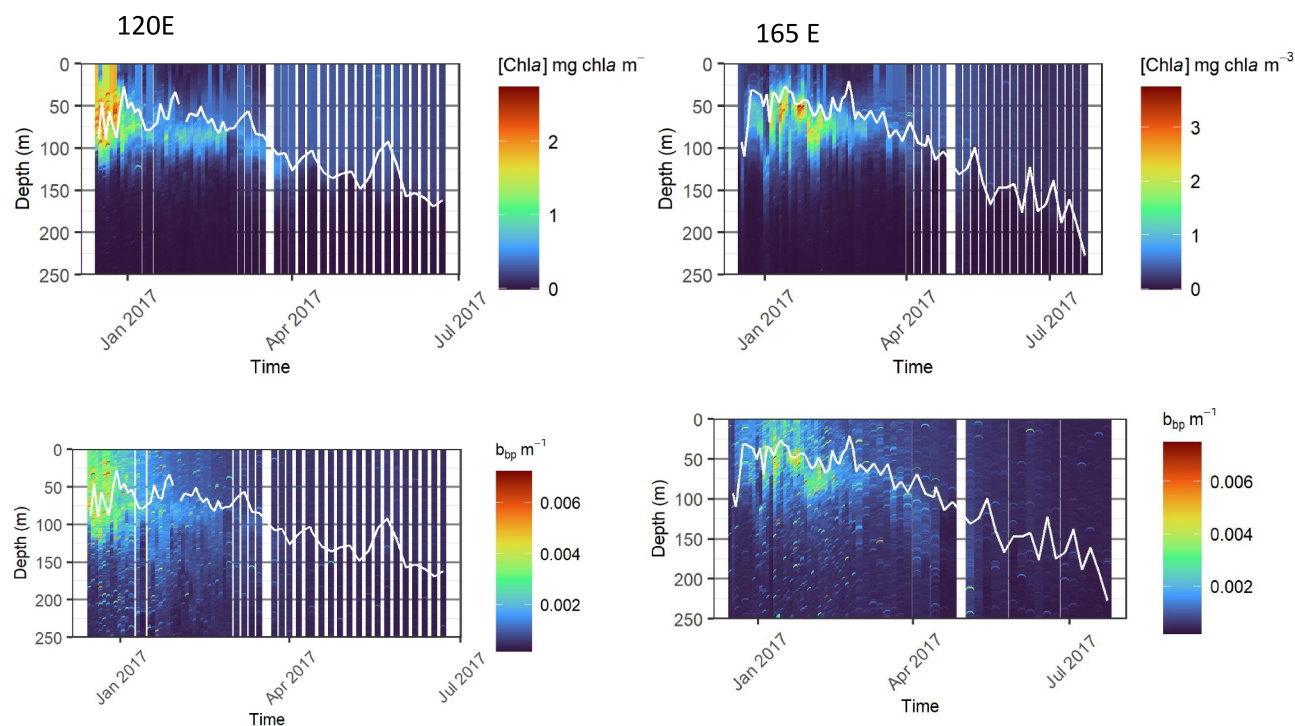


Figure 12. Time-series observations of the DCM and DBM from Cornec, Claustre, et al. (2021) for the two floats within the IPFZ featured in Figure 11. The sampling frequency for both floats was every 2 days before March 2017, 4 days during March 2017, and 5 days after March 2017. The mixed layer depth is denoted with a white line.

Joint Global Ocean Flux Study (JGOFS) process study. In the lab, Meyerink et al. (2017) measured a half-saturation constant of $11 \mu\text{mol L}^{-1}$ for the diatom *Proboscia inermis* (observed in the 56°S DCM/DBM feature) and $9 \mu\text{mol L}^{-1}$ for *Eucampia antarctica* when grown under Fe-replete conditions, so silicate availability may be an issue for larger diatoms that reside in the DCM (Figure S7 in Supporting Information S1). Thus, increased silicate availability at depth may be a driver, along with Fe supply via recycling, for the formation of a DCM in the IPFZ. Our proposed drivers bring together prior suggestions for the role of silicate resupply (Parslow et al., 2001) and “irregular fertilization” of Fe (Cornec, Claustre, et al., 2021), but go one step further by identifying a putative mechanism for sustained Fe supply via recycled rather than new Fe (from the ferricline) that may be linked to the presence of the subsurface ammonium maximum.

4.4. Wider Distribution of DCMs/DBMs

DCMs/DBMs are typically sampled opportunistically, and hence most observational records are based on a small number of CTD profiles (Baldry et al., 2020) along with a wider extrapolation of oceanographic snapshots of DCM features across regions (e.g., Parslow et al., 2001). The availability of both the towbody (night-time only) and BGC-ARGO observations enable us to assess the wider distribution of the DCM/DBM both around our sampling sites, and for the BGC-ARGO float after the vessel departed the sites. The tow-body sections reveal that the water mass associated with the IPFZ extended by at least a 15 km radius around our sampling site at $\sim 56^\circ\text{S}$ (Figure 6). There is a strong coherence along each towbody section in the depth and thickness (~ 20 m) of both the DCM and DBM. Any small variations in the DCM’s depth or thickness were mirrored by that for the DBM, likely reflecting small variations in the depth of the seasonal mixed layer in this region. The C:Chlorophyll ratio of the subsurface feature was also relatively constant along each section and was several-fold lower than that in the overlying waters. The ratios in the upper ocean were typical of those observed in the seasonal mixed layer (Riemann et al., 1989). In contrast, the C:Chlorophyll ratios in the DCM were typical of regions with more subsurface carbon at depth than chlorophyll (Taylor et al., 1997). At the 58°S site, the presence of subsurface features was more variable, reflecting their development toward the end of our site occupation (Figure 7 and Figure S8 in Supporting Information S1).

The wider distribution of the DCM/DBM can also be explored, in part, using the BGC-ARGO high-resolution time-series (Figures 8 and 9) as the float remained both in the vicinity of the 56°S site (Figure S1a in Supporting Information S1) and within the water mass characteristics of the IPFZ. For example, the T_{min} layer at depth is conspicuous in the float time-series observations (Figure 8a). Again, a coherent DCM co-located with a DBM is evident for several months (Figures 9a and 9b). As for the towbody, lower C:Chlorophyll ratios were evident in the subsurface feature when compared to those in the overlying waters from profiles obtained under darkness (interspersed with noon profiles, as is evident from Figures 9c and 9d). The multi-month float record also provides insights into the DCM longevity and its eventual decline.

4.5. Fate of the DCM/DBM

Most prior studies of DCMs/DBMs in the S. Oceans have been opportunistic “snapshots” (e.g., Parslow et al., 2001; Trull et al., 2001). Insights into the lifetime of such features have therefore come from inference. For example, Parslow et al. (2001) observed DCMs from November to March, but they were prescribed profiles as part of WOCE and JGOFS transects that straddled multiple years. A recent compilation of DCMs from Southern Ocean BGC-ARGO floats reveals several cases in which a DCM/DBM was repeatedly observed (Cornec, Claustre, et al., 2021; this study Figures 11 and 12). These studies provide more examples of extended observations of the DCM and DBM to compare with those from January 2021 to May 2021 when the decline of the DCM was evident (Figure 9).

The sampling of a DCM in March within the IPFZ, south of Australia, by Parslow et al. (2001) pointed to a feature in decline, as evinced by empty diatom frustules in the DCM (Kopczynska et al., 2001), and no difference between the photosynthetic metric alpha (slope of the PE curve) within the DCM relative to the overlying waters. In contrast, higher alpha values (indicative of photoacclimation) were reported in January (summer) DCMs sampled by Parslow et al. (2001). A major unknown from the Parslow et al. (2001) study is whether the DCMs they observed were also representative of DBMs, but there are some suggestions from the relatively high NPP within the DCM features that they may also have been DBMs. The longer time records from Cornec, Claustre, et al. (2021) reveal for two floats within the IPFZ (Figures 11 and 12) that both DCMs and DBMs were evident in BGC-ARGO time-series observations below the seasonal mixed layer to a depth of ~80 m (i.e., 30 m thick features) in the vicinity of 120°E (WMO # 6901581) for ~55 days (30 December 2016 to 24 February 2017) and near 165°E (WMO # 6901004) for ~60 days (29 Dec 2016 to 03 March 2017). The fate of these features—a decline in late March and no evidence of a particle export pulse—appears similar to that of the DCM/DBM recorded by the float near the 56°S site in the present study (Figure 9 cf. Figure 12).

At the 56°S site, the subsurface feature persisted until mid-April 2021, with coherence between the thickness and depth strata of the DCM and DBM, along with little change in C:Chlorophyll ratios in the subsurface feature (Figure 9). The latter is indicative of a healthy population of diatoms and hence a strong indication of a region in which NPP persisted, albeit at lower rates (see Figure 3). The decline of the DCM was relatively abrupt (likely driven by vanishingly low light levels, Figure S5b in Supporting Information S1), and there was no evidence of a late-season fall-out of the large diatoms to depth, as has been speculated by Queguiner (2013) and Kemp et al. (2000). The decline was likely driven by a decrease in underwater solar radiation, which declines markedly in this polar region to <3 μmol photons m⁻² d⁻¹ (Figure S9 in Supporting Information S1). Prior to April, there was no clear trend in the column-integrated irradiances recorded on profiles by the float at 56°S (Figure S9a in Supporting Information S1). What was the fate of the large diatoms within the DCM?

During our occupation of the 56°S site in late December 2020/early January 2021, there was evidence of grazing by salp swarms but no change in the DCM characteristics over this period. Microscopic analysis of dissected salp guts revealed some large diatoms, but they were intact and likely passed through the gut (Figure S13 in Supporting Information S1). The likely fate of the diatoms within the DCM may have been a slow but continuous export of a fraction of the assemblage, given that the feature appeared stable and viable for months (Figure 9), as opposed to an export pulse which would have been conspicuous from the bio-optical sensors on the float (see Figure 10). Such a constant and low export flux may have been driven by self-regulation of the thickness and integrated chlorophyll (a community response analogous to the cellular self-shading “package effect”) within the DCM (see Lande et al., 1989). As stated earlier, the ability of large polar diatoms to increase their light-harvesting antennae (a mechanism that requires no additional Fe, Strzepek et al., 2012, 2019) may have exacerbated this chlorophyll “package” effect leading to their vertical export.

There is some evidence of such a low but constant export flux from chlorophyll fluorescence and backscatter from January to April 2021 (Figure 10). However, these downward fluxes are more evident for backscatter than for chlorophyll fluorescence, suggesting chlorotic cells with declining chlorophyll relative to carbon. Such chlorotic cells would be linked to their senescence after less than a week (Strzepek et al., 2012) based on observations of lab-cultured *S. Ocean* polar diatoms under high Fe but low light conditions (i.e., reflecting the environment within the DCM/DBM). These observations help inform on the wider functional role of the DCM and DBM.

4.6. Ecological and Biogeochemical Roles of the DCM/DBM

Recent reviews of *S. Ocean* NPP (Pinkerton et al., 2021) and biogeochemistry (Henley et al., 2020) suggest that DCMs play important ecological and/or biogeochemical roles based on particle export. Our suite of data sets from diverse observational platforms offers insights into the wider roles of DCMs/DBMs. The co-location of both the DCM and DBM, which is mainly associated with diatoms, along with its multi-month persistence suggests that it is a subsurface niche that develops because of the decline of the surface mixed layer phytoplankton community (Figure S10 and Table S1 in Supporting Information S1) following resource limitation by both silicate and Fe. The surface waters appear, based on the BGC-ARGO float records (Figure 9), to have low and constant chlorophyll and C concentrations that characterize a seasonal High-Nutrient Low-Chlorophyll province (Arrigo et al., 2015; Boyd et al., 2000; Boyd & Law, 2001). The development of the subsurface diatom community will have ramifications for the cycles of Fe, silicate and C in particular. The diatom community appears to be driven by the availability of silicate below the seasonal mixed layer along with Fe derived from recycling rather than new sources. NPP is relatively low—we measured $0.2 \mu\text{mol L}^{-1} \text{d}^{-1}$ in the DCM. Other studies have estimated NPP from DCMs, but these are based on snapshots from short station occupations. Parslow et al. (2001) reported a maximum rate of NPP of $0.25 \mu\text{mol L}^{-1} \text{d}^{-1}$ (equivalent to the daily “production” of 4×10^4 (*E. antarctica*) to 5.5×10^4 (*P. inermis*) diatom cells L^{-1} (based on Supporting Information in Strzepek et al., 2019) in the DCM in October and January, decreasing to $<0.1 \mu\text{mol L}^{-1} \text{d}^{-1}$ in March.

Prior NPP estimates (Parslow et al., 2001) did not take into consideration the thickness of the stratum associated with the DCM/DBM. Based on robust estimates, from our three observational approaches, we can extrapolate this NPP rate over the ~ 25 m thick feature (Figure 9), resulting in a column integral of $5.0 \text{ mmol m}^{-2} \text{d}^{-1}$. Further extrapolation, based on little change in C:Chlorophyll ratios which is indicative of relatively healthy cells, to a month suggests that an NPP of 150 mmol m^{-2} monthly could be contributed by this feature which persisted for 3 months (Figure 9). The fate of this additional carbon is unknown but based on the bio-optical sensor time-series (Figure 10), it could be a “slow trickle” of exported particles to depth. Herbivory data during the ship occupation of the 56°S site suggest that salps can ingest but not consume these large diatoms (Figure S13 in Supporting Information S1). Thus, it is possible that most losses can be attributed to export rather than secondary consumption, leading to a “slow trickle” of up to $150 \text{ mmol POC m}^{-2}$ each month from ~ 90 m depth.

Is there a biogeographic province for *S. Ocean* DCM/DBMs? Our findings, along with those from Parslow et al. (2001) south of Australia, and several of the floats featured in the Corneec, Claustre, et al. (2021) global DCM analysis, but re-examined in detail here (Figure 11), suggest that the IPFZ may be such a region. It can provide both silicate at depth and potentially in situ Fe recycling by microbes associated with the subsurface ammonium maximum. However, additional insights come from observations from the waters north and south of the IPFZ. To the north, in the subantarctic, which also has seasonal silicate limitation (Hutchins et al., 2001), there is no evidence of a DCM or DBM, suggesting that alleviation of similar limitation at depth alone may not result in a DCM/DBM. To the south of the IPFZ, the SOIREE site (Trull et al., 2001) was south of the southern branch of the Polar Front in eastward flowing Antarctic Circumpolar Current waters. This site was characterized by a T_{min} layer (but there are no ammonium data) and Figure 9 in Trull et al. (2001) reveals that silicate is most likely never fully depleted in surface waters at 61°S . Thus, the physico-chemical characteristics of the IPFZ may play a key role by being both silicate and Fe depleted in surface waters yet being able to provide both nutrients in the subsurface, but via different mechanisms—from the nutricline for silicate and potentially via recycling for Fe. The IPFZ thus provides an interesting testbed to see if it represents a province in which both DCM and DBM are co-located, as opposed to other regions where only DCMs comprising photoacclimated cells are evident (Baldry et al., 2020; Carranza et al., 2018; Corneec, Claustre, et al., 2021).

Data Availability Statement

All observations and data presented in the Figures and Supporting Figures are available via Boyd and Rohr (2023).

Acknowledgments

Many thanks to the scientific staff and crew of the RV Investigator who safely and successfully navigated us around the three SOLACE sites in the Southern Ocean. We acknowledge the use of the CSIRO Marine National Facility (<https://ror.org/01mae9353>) and grant of sea time to RV Investigator in undertaking this research. Open access publishing facilitated by University of Tasmania, as part of the Wiley - University of Tasmania agreement via the Council of Australian University Librarians.

References

- Allen, J. T., Brown, L., Sanders, R., Moore, C. M., Mustard, A., Fielding, S., et al. (2005). Diatom carbon export enhanced by silicate upwelling in the northeast Atlantic. *Nature*, *437*(7059), 728–732. <https://doi.org/10.1038/nature03948>
- Ardyna, M., Lacour, L., Sergi, S., d'Ovidio, F., Sallée, J. B., Rembauville, M., et al. (2019). Hydrothermal vents trigger massive phytoplankton blooms in the Southern Ocean. *Nature Communications*, *10*(1), 2451. <https://doi.org/10.1038/s41467-019-09973-6>
- Argo (2000). Argo float data and metadata from Global Data Assembly Centre (Argo GDAC). *SEANOE*. <https://doi.org/10.17882/42182>
- Arrigo, K. R., van Dijken, G. L., & Strong, A. L. (2015). Environmental controls of marine productivity hot spots around Antarctica. *Journal of Geophysical Research: Oceans*, *120*(8), 5545–5565. <https://doi.org/10.1002/2015JC010888>
- Baldry, K., Stratton, P. G., Hill, N. A., & Boyd, P. W. (2020). Subsurface chlorophyll-a maxima in the southern ocean. *Frontiers in Marine Science*, *7*, 671. <https://doi.org/10.3389/fmars.2020.00671>
- Barbieux, M., Uitz, J., Gentili, B., Pasqueron De Fommervault, O., Mignot, A., Poteau, A., et al. (2019). Bio-optical characterization of subsurface chlorophyll maxima in the Mediterranean Sea from a Biogeochemical-Argo float database. *Biogeosciences*, *16*(6), 1321–1342. <https://doi.org/10.5194/bg-16-1321-2019>
- Behrenfeld, M. J., Boss, E., Siegel, D. A., & Shea, D. M. (2005). Carbon-based ocean productivity and phytoplankton physiology from space. *Global Biogeochemical Cycles*, *19*(1), GB1006. <https://doi.org/10.1029/2004gb002299>
- Biermann, L., Guinet, C., Bester, M., Brierley, A., & Boehme, L. (2015). An alternative method for correcting fluorescence quenching. *Ocean Science*, *11*(1), 83–91. <https://doi.org/10.5194/os-11-83-2015>
- Bock, N., Subramaniam, A., Juhl, A. R., Montoya, J., & Duhamel, S. (2022). Quantifying per-cell chlorophyll a in natural picophytoplankton populations using fluorescence activated cell sorting. *Frontiers in Marine Science*, *9*, 850646. <https://doi.org/10.3389/fmars.2022.850646>
- Böckmann, S., Koch, F., Meyer, B., Pausch, F., Iversen, M., Driscoll, R., et al. (2021). Salp fecal pellets release more bioavailable iron to Southern Ocean phytoplankton than krill fecal pellets. *Current Biology*, *31*(13), 2737–2746.e3. <https://doi.org/10.1016/j.cub.2021.02.033>
- Boyd, P., & Rohr, T. (2023). Data for Boyd (2023) 'Controls on polar Southern Ocean deep chlorophyll maxima: Viewpoints from multiple observational platforms' [Dataset]. *Institute for Marine and Antarctic Studies (IMAS), University of Tasmania (UTAS)*. <https://doi.org/10.25959/boyd-sodcm23>
- Boyd, P. W., & Abraham, E. R. (2001). Iron-mediated changes in phytoplankton photosynthetic competence during SOIREE. *Deep-Sea Res. (II Top. Stud. Oceanogr.)*, *48*(11–12), 2529–2550. [https://doi.org/10.1016/s0967-0645\(01\)00007-8](https://doi.org/10.1016/s0967-0645(01)00007-8)
- Boyd, P. W., Doney, S. C., EllwoodFourquez, S. M. J. M., Ellwood, M. J., Fourquez, M., Nunn, B. L., et al. (2022). Transitioning global change experiments on Southern Ocean phytoplankton from lab to field settings: Insights and challenges. *Limnology & Oceanography*, *67*(9), 1911–1930. <https://doi.org/10.1002/lno.12175>
- Boyd, P. W., & Law, C. S. (2001). The southern ocean iron release experiment (SOIREE)—Introduction and summary. *Deep-Sea Res II*, *48*(11–12), 2425–2438. [https://doi.org/10.1016/s0967-0645\(01\)00002-9](https://doi.org/10.1016/s0967-0645(01)00002-9)
- Boyd, P. W., Watson, A. J., Law, C. S., Abraham, E. R., Trull, T., Murdoch, R., et al. (2000). A mesoscale phytoplankton bloom in the polar Southern Ocean stimulated by iron fertilization. *Nature*, *407*(6805), 695–702. <https://doi.org/10.1038/35037500>
- Boyer Montégut, C. d., Madec, G., Fischer, A. S., Lazar, A., & Iudicone, D. (2004). Mixed layer depth over the global ocean: An examination of profile data and a profile-based climatology. *Journal of Geophysical Research*, *109*(C12), C12003. <https://doi.org/10.1029/2004JC002378>
- Briggs, N., Dall'Olmo, G., & Claustre, H. (2020). Major role of particle fragmentation in regulating biological sequestration of CO₂ by the oceans. *Science*, *367*(6479), 791–793. <https://doi.org/10.1126/science.aay1790>
- Brezinski, M. A., Pride, C. J., Franck, V. M., Sigman, D. M., Sarmiento, J. L., Matsumoto, K., et al. (2002). A switch from Si(OH)₄ to NO₃⁻ depletion in the glacial Southern Ocean. *Geophysical Research Letters*, *29*(12), 5-1–5-4. <https://doi.org/10.1029/2001GL014349>
- Carranza, M. M., Gille, S. T., Franks, P. J. S., Johnson, K. S., Pinkel, R., & Girtton, J. B. (2018). When mixed layers are not mixed. storm-driven mixing and biooptical vertical gradients in mixed layers of the southern ocean. *Journal of Geophysical Research: Oceans*, *123*(10), 7264–7289. <https://doi.org/10.1029/2018JC014416>
- Cornec, M., Claustre, H., Mignot, A., Guidi, L., Lacour, L., Poteau, A., et al. (2021). Deep chlorophyll maxima in the global ocean: Occurrences, drivers and characteristics. *Global Biogeochemical Cycles*, *35*(4), e2020GB006759. <https://doi.org/10.1029/2020GB006759>
- Cornec, M., Laxenaire, R., Speich, S., & Claustre, H. (2021). Impact of mesoscale eddies on deep chlorophyll maxima. <https://doi.org/10.1029/2021GL093470>
- Cullen, J. J. (1982). The deep chlorophyll maximum: Comparing vertical profiles of chlorophyll a. *Canadian Journal of Fisheries and Aquatic Sciences*, *39*(5), 791–803. <https://doi.org/10.1139/f82-108>
- Cullen, J. J. (2015). Subsurface chlorophyll maximum layers: Enduring enigma or mystery solved? *Annual Review of Marine Science*, *7*(1), 207–239. <https://doi.org/10.1146/annurev-marine-010213-135111>
- Dong, S., Gille, S. T., Sprintall, J., et al. (2007). An assessment of the southern ocean mixed layer heat budget. *Journal of Climate*, *20*(17), 4425–4442. <https://doi.org/10.1175/JCL14259.1>
- Du Plessis, M. D., Swart, S., Biddle, L. C., Giddy, I. S., Monteiro, P. M. S., Reason, C. J. C., et al. (2022). The daily-resolved southern ocean mixed layer: Regional contrasts assessed using glider observations. *Journal of Geophysical Research: Oceans*, *127*(4), e2021JC017760. <https://doi.org/10.1029/2021jc017760>
- Ellwood, M. J., Strzepek, R., Chen, X., Trull, T. W., & Boyd, P. W. (2020b). Some observations on the biogeochemical cycling of zinc in the Australian sector of the Southern Ocean: A dedication to Keith Hunter. *Marine and Freshwater Research*, *71*(3), 355–373. <https://doi.org/10.1017/mf19200>
- Ellwood, M. J., Strzepek, R. F., Stratton, P. G., Trull, T. W., Fourquez, M., & Boyd, P. W. (2020a). Distinct iron cycling in a Southern Ocean eddy. *Nature Communications*, *11*(1), 825. <https://doi.org/10.1038/s41467-020-14464-0>
- Gomi, Y., Fukuchi, M., & Taniguchi, A. (2010). Diatom assemblages at subsurface chlorophyll maximum layer in the eastern Indian sector of the Southern Ocean in summer. *Journal of Plankton Research*, *32*(7), 1039–1050. <https://doi.org/10.1093/plankt/fbq031>
- Henley, S., Cavan, E. L., Fawcett, S. E., Kerr, R., Monteiro, T., Sherrell, R. M., et al. (2020). Changing biogeochemistry of the Southern Ocean and its ecosystem implications. *Frontiers in Marine Science*, *7*, 581. <https://doi.org/10.3389/fmars.2020.00581>

- Hogle, S. L., Dupont, C. L., Hopkinson, B. M., King, A. L., Buck, K. N., Roe, K. L., et al. (2018). Pervasive iron limitation at subsurface chlorophyll maxima of the California Current. *PNAS*, *115*(52), 13300–13305. <https://doi.org/10.1073/pnas.1813192115>
- Holm-Hansen, O., & Hewes, C. D. (2004). Deep chlorophyll-a maxima (DCMs) in Antarctic waters: I. Relationships between DCMs and the physical, chemical, and optical conditions in the upper water column. *Polar Biology*, *27*(11), 699–710. <https://doi.org/10.1007/s00300-004-0641-1>
- Holte, J., & Talley, L. (2009). A new algorithm for finding mixed layer depths with applications to argo data and subantarctic mode water formation. *Journal of Atmospheric and Oceanic Technology*, *26*(9), 1920–1939. <https://doi.org/10.1175/2009JTECH0543.1>
- Hopkinson, B. M., & Barbeau, K. A. (2008). Interactive influences of iron and light limitation on phytoplankton at subsurface chlorophyll maxima in the eastern North Pacific. *Limnology & Oceanography*, *53*(4), 1303–1318. <https://doi.org/10.4319/lo.2008.53.4.1303>
- Hoppe, C. J. M. (2021). Always ready? Primary production of Arctic phytoplankton at the end of the polar night. *Limnology and Oceanography Letters*, *7*(2022), 167–174. <https://doi.org/10.1002/lo2.10222>
- Hutchins, D. A., Crossley, A. C., DiTullio, G. R., Griffiths, F. B., Boyd, P. W., Queguiner, B., et al. (2001). Control of phytoplankton growth by iron and silicic acid availability in the Subantarctic Southern Ocean: Experimental results from the SAZ project. *Journal of Geophysical Research*, *106*(2000), 31573–31583. <https://doi.org/10.1029/2000JC000348>
- Johnson, K. S., Plant, J. N., Coletti, L. J., Jannasch, H. W., Sakamoto, C. M., Riser, S. C., et al. (2017). Biogeochemical sensor performance in the SOCCOM profiling float array. *Journal of Geophysical Research: Oceans*, *122*(8), 6416–6436. <https://doi.org/10.1002/2017JC012838>
- Kemp, A. E. S., Pike, J., Pearce, R. B., & Lange, C. B. (2000). The “Fall dump” – A new perspective on the role of a “shade flora” in the annual cycle of diatom production and export flux. *Deep-Sea Research Part II Topical Studies in Oceanography*, *47*(9–11), 2129–2154. [https://doi.org/10.1016/S0967-0645\(00\)00019-9](https://doi.org/10.1016/S0967-0645(00)00019-9)
- Kennedy, F., Martin, A., Bowman, J. P., Wilson, R., & McMin, A. (2019). Dark metabolism: A molecular insight into how the Antarctic sea-ice diatom *Fragilariopsis cylindrus* survives long-term darkness. *New Phytologist*, *223*(2), 675–691. <https://doi.org/10.1111/nph.15843>
- Kirk, J. T. O. (1994). *Light and photosynthesis in aquatic ecosystems*. Cambridge University Press.
- Klunder, M. B., Laan, P., Middag, R., De Baar, H. J., & van Ooijen, J. C. (2011). Dissolved iron in the Southern Ocean (Atlantic sector). *Deep-Sea Research Part II Topical Studies in Oceanography*, *58*(25–26), 2678–2694. <https://doi.org/10.1016/j.dsr2.2010.10.042>
- Kopczynska, E. E., Dehairs, F., Elskens, M., & Wright, S. (2001). Phytoplankton and microzooplankton variability between the Subtropical and Polar Fronts south of Australia: Thriving under regenerative and new production in late summer. *Journal of Geophysical Research: Oceans*, *106*(C12), 31597–31609. <https://doi.org/10.1029/2000JC000278>
- Kwong, L. E., Henschke, N., Pakhomov, E. A., Everett, J. D., & Suthers, I. M. (2020). Mesozooplankton and micronekton active carbon transport in contrasting eddies. *Frontiers in Marine Science*, *6*. <https://doi.org/10.3389/fmars.2019.00825>
- Lande, R., Li, W. K., Horne, E. P. W., & Wood, M. (1989). Phytoplankton growth rates estimated from depth profiles of cell concentration and turbulent diffusion. *Deep-Sea Research*, *36*(8), 1141–1159. [https://doi.org/10.1016/0198-0149\(89\)90097-6](https://doi.org/10.1016/0198-0149(89)90097-6)
- Latour, P., Eggins, S., van der Merwe, P., Bach, L., Boyd, P. W., Ellwood, M., et al. (2023). Characterization of a Southern Ocean deep chlorophyll maximum: Response of phytoplankton to light, iron and manganese enrichment. *Limnology and Oceanography Letters*. <https://doi.org/10.1002/lo2.10366>
- Marañón, E., Van Wambeke, F., Uitz, J., Boss, E. S., Dimier, C., Dinasquet, J., et al. (2021). Deep maxima of phytoplankton biomass, primary production and bacterial production in the Mediterranean Sea. *Biogeosciences*, *18*(5), 1749–1767. <https://doi.org/10.5194/bg-18-1749-2021>
- Mdutyana, M., Thomalla, S. J., Philibert, R., Ward, B. B., & Fawcett, S. E. (2020). The seasonal cycle of nitrogen uptake and nitrification in the Atlantic sector of the Southern Ocean. *Global Biogeochemical Cycles*, *34*(7), e2019GB006363. <https://doi.org/10.1029/2019GB006363>
- Meyerink, S. W., Ellwood, M. J., Maher, W. A., Dean Price, G., & Strzepek, R. F. (2017). Effects of iron limitation on silicon uptake kinetics and elemental stoichiometry in two Southern Ocean diatoms, *Eucampia Antarctica* and *Proboscia inermis*, and the temperate diatom *Thalassiosira pseudonana*. *Limnology & Oceanography*, *62*(6), 2445–2462. <https://doi.org/10.1002/lno.10578>
- Nelson, D. M., Brzezinski, M. A., Sigmon, D. E., & Frank, V. M. (2001). A seasonal progression of Si limitation in the Pacific sector of the Southern Ocean. *Deep-Sea Res. II*, *48*(19–20), 3973–3995. [https://doi.org/10.1016/S0967-0645\(01\)00076-5](https://doi.org/10.1016/S0967-0645(01)00076-5)
- Pasche, E. (1973). Silicon and the ecology of marine plankton diatoms. I. *Thalassiosira Pseudonana* (Cyclotella Nana) Grown in a chemostat with silicate as limiting nutrient. *Marine Biology*, *19*(2), 117–126. <https://doi.org/10.1007/BF00353582>
- Parslow, J. S., Boyd, P. W., Rintoul, S. R., & Griffiths, F. B. (2001). A persistent subsurface chlorophyll maximum in the Interpolar Frontal Zone south of Australia: Seasonal progression and implications for phytoplankton-light-nutrient interactions. *Journal of Geophysical Research*, *106*(C12), 31543–31557. <https://doi.org/10.1029/2000jc000322>
- Pinkerton, M. H., Boyd, P. W., Deppeler, S., Hayward, A., Höfer, J., & Moreau, S. (2021). Evidence for the impact of climate change on primary producers in the southern ocean. *Front. Ecol. Evol.*, *9*, 592027. <https://doi.org/10.3389/fevo.2021.592027>
- Pollehne, F., Klein, B., & Zeitzschel, B. (1993). Low light adaptation and export production in the deep chlorophyll maximum layer in the northern Indian Ocean. *Deep Sea Research Part II: Topical Studies in Oceanography*, *40*(3), 737–752. [https://doi.org/10.1016/0967-0645\(93\)90055-R](https://doi.org/10.1016/0967-0645(93)90055-R)
- Queguiner, B. (2013). Iron fertilization and the structure of planktonic communities in high nutrient regions of the Southern Ocean. *Deep Sea Research Part II: Topical Studies in Oceanography*, *90*, 43–54. <https://doi.org/10.1016/j.dsr2.2012.07.024>
- Rees, C., Pender, L., Sherrin, K., Schwanger, C., Hughes, P., Tibben, S., et al. (2018). Methods for reproducible shipboard SFA nutrient measurement using RMNS and automated data processing. *Limnology & Oceanography: Methods, December*, *LOM3.10294*, *17*(1), 25–41. <https://doi.org/10.1002/lom3.10294>
- Riemann, B., Simonsen, P., & Stensgaard, L. (1989). The carbon and chlorophyll content of phytoplankton from various nutrient regimes. *Journal of Plankton Research*, *11*(5), 1037–1045. <https://doi.org/10.1093/plankt/11.5.1037>
- Schmechtig, C., Boss, E., Briggs, N., Claustre, H., Dall’Omo, G., & Poteau, A. (2019). BGC Argo quality control manual for particles back-scattering. <https://doi.org/10.13155/60262>
- Schmechtig, C., Claustre, H., Poteau, A., & D’Ortenzio, F. (2014). Bio-argo quality control manual for the Chlorophyll-A concentration. <https://doi.org/10.13155/35385>
- Sigmon, D. E., Nelson, D. M., & Brzezinski, M. A. (2002). The Si cycle in the Pacific sector of the Southern Ocean: Seasonal diatom production in the surface layer and export to the deep sea. *Deep Sea Res. Pt II*, *49*(9–10), 1747–1763. [https://doi.org/10.1016/S0967-0645\(02\)00010-3](https://doi.org/10.1016/S0967-0645(02)00010-3)
- Smetacek, V. (2001). A watery arms race. *Nature*, *411*(6839), 745. <https://doi.org/10.1038/35081210>
- Strutton, P. G., Trull, T. W., Phillips, H. E., Duran, E. R., & Pump, S. (2023). Biogeochemical Argo floats reveal the evolution of subsurface chlorophyll and particulate organic carbon in southeast Indian Ocean eddies. *Journal of Geophysical Research: Oceans*, *128*(4), e2022JC018984. <https://doi.org/10.1029/2022JC018984>
- Strzepek, R. F., Boyd, P. W., & Sunda, W. G. (2019). Photosynthetic adaptation to low iron, light, and temperature in Southern Ocean phytoplankton. *Proceedings of the National Academy of Sciences of the United States of America*, *116*(10), 4388–4393. <https://doi.org/10.1073/pnas.1810886116>

- Strzepek, R. F., Hunter, K. A., Frew, R. D., Harrison, P. J., & Boyd, P. W. (2012). Iron–light interactions differ in Southern Ocean phytoplankton. *Limnology & Oceanography*, *57*(4), 1182–1200. <https://doi.org/10.4319/lo.2012.57.4.1182>
- Taylor, A. H., Geider, R. J., & Gilbert, F. J. H. (1997). Seasonal and latitudinal dependencies of phytoplankton carbon-to-chlorophyll a ratios: Results of a modeling study. *Marine Ecology Progress Series*, *152*(1–3), 51–66. <https://doi.org/10.3354/meps152051>
- Thomalla, S. J., Moutier, W., Ryan-Keogh, T. J., Gregor, L., & Schütt, J. (2018). An optimized method for correcting fluorescence quenching using optical backscattering on autonomous platforms. *Limnology and Oceanography: Methods*, *16*(2), 132–144. <https://doi.org/10.1002/lom3.10234>
- Trull, T., Rintoul, S. R., Hadfield, M., & Abraham, E. R. (2001). Circulation and seasonal evolution of polar waters south of Australia: Implications for iron fertilization of the Southern Ocean. *Deep-Sea Research II*, *48*(11–12), 2439–2466. [https://doi.org/10.1016/s0967-0645\(01\)00003-0](https://doi.org/10.1016/s0967-0645(01)00003-0)
- Trull, T. W., Passmore, A., Davies, D. M., Smit, T., Berry, K., & Tilbrook, B. (2018). Distribution of planktonic biogenic carbonate organisms in the Southern Ocean south of Australia: A baseline for ocean acidification impact assessment. *Biogeosciences*, *15*(1), 31–49. <https://doi.org/10.5194/bg-15-31-2018>
- Uchida, T., Balwada, D., Abernathy, R. P., McKinley, G. A., Smith, S. K., & Lévy, M. (2020). Vertical eddy iron fluxes support primary production in the open Southern Ocean. *Nature Communications*, *11*(1), 1125. <https://doi.org/10.1038/s41467-020-14955-0>
- Xing, X., Claustre, H., Blain, S., D'Ortenzio, F., Antoine, D., Ras, J., & Guinet, C. (2012). Quenching correction for in vivo chlorophyll fluorescence acquired by autonomous platforms: A case study with instrumented elephant seals in the Kerguelen region (Southern Ocean). *Limnology Oceanogr. Methods*, *1*(2012), 483–495. <https://doi.org/10.4319/lom.2012.10.483>
- Yool, A., & Tyrrell, T. (2003). Role of diatoms in regulating the ocean's silicon cycle. *Global Biogeochemical Cycles*, *17*(4), 1103. <https://doi.org/10.1029/2002gb002018>
- Wong, A., Keeley, R., & Carval, T., & the Argo Data Management Team. (2023). Argo quality control manual for CTD and trajectory data. <https://doi.org/10.13155/33951>